Enhancing Functionalities of Engineered Skeletal Muscle Tissues by Recreating Natural Environmental Cues

by

Hyeon Yu Kim

B.S., Mechanical Engineering,
Korea Advanced Institute of Science and Technology (2012)
S.M., Mechanical Engineering,
Massachusetts Institute of Technology (2014)

Submitted to the Department of Mechanical Engineering
in partial fulfillment of the requirements for the degree of

Doctor of Philosophy in Mechanical Engineering

at the

MASSACHUSETTS INSTITUTE OF TECHNOLOGY

June 2019

Signature redacted

Author .....
Department of Mechanical Engineering
May 20, 2019

Certified by ..... Signature redacted .....
H. Harry Asada
Ford Professor of Engineering
Thesis Supervisor

Accepted by ..... Signature redacted .....
Nicolas Hadjiconstantinou
Chairman, Department Committee on Graduate Theses

Enhancing Functionalities of Engineered Skeletal Muscle Tissues by Recreating Natural Environmental Cues

by

Hyeon Yu Kim

Submitted to the Department of Mechanical Engineering
on May 20, 2019, in partial fulfillment of the
requirements for the degree of
Doctor of Philosophy in Mechanical Engineering

Abstract

Engineered skeletal muscle tissue is a three-dimensional contractile tissue made from muscle cells and the extracellular matrix (ECM). It can be used as a drug testing platform or an implantable tissue, but its practical use has been limited by inferior contractile performance and small size compared to natural muscles. This thesis aims to implement environmental cues and essential elements of natural muscles to improve the contractile performance and increase its size beyond the diffusion limit. Firstly, inspired by the observation that the natural muscles are exposed to electric potentials from neurons in combination with mechanical stretching from surrounding muscles, a new muscle training system was developed to apply coordinated electrical and mechanical stimulation. Both the experimental results and the mechanistic model suggest the combined stimulation reorients the ECM fibers in such a way that the parallel ECM stiffness is reduced, while the serial ECM stiffness is increased, which reduces resistance to muscle contraction and increases force transmission in the engineered muscles, respectively. Secondly, large-sized natural muscles are fully vascularized so that oxygen and nutrients can be supplied. However, vascularization of the engineered skeletal muscle has been challenging because the microenvironmental requirement for differentiating myoblasts is incompatible with the one for culturing endothelial cells. In contrast, the natural muscle tissue has a compartment structure, where endothelial cells are exposed to blood plasma, while myoblasts are surrounded by interstitial fluid. In this thesis, we modeled the natural fluid compartments by creating an *in vitro* perfusable vasculature running through a skeletal muscle tissue with physiologic cell density. The tissue is designed to have a coaxial tubular shape with a perfusable vasculature at the center. Through the *in vitro* fluid compartments, endothelial cells are exposed to endothelial cell growth medium running through the vascular channel, and the skeletal muscle cells are surrounded by muscle differentiation medium. By using this platform, engineered muscle tissue was successfully scaled up from microscale to subcentimeter scale. This platform also enabled to show that coculturing with the two separate media from an early stage of muscle differentiation leads to increased contractile force, thicker myotubes, and more muscle differentiation

compared to using a single coculture medium. Furthermore, the engineered skeletal muscles were further vascularized by inducing angiogenic sprouting from the vascular channel penetrating into the muscle tissue. This thesis will contribute to utilizing engineered skeletal muscles in practical applications with improved functionalities and provide a new model to study heterotypic cell-cell interactions in skeletal muscle tissues.

Thesis Supervisor: H. Harry Asada
Title: Ford Professor of Engineering

Acknowledgments

First of all, I would like to thank Professor Asada, who gave me an opportunity to study in the d'Arbeloff lab and taught me a logical way of thinking. Without his dedicated support and guidance, this thesis could never have been completed. I sincerely thank him for being a truly great mentor for all aspects of my life as well as my thesis advisor. I would also like to thank Professor Kamm for providing me with constructive research advice and for expanding my research scope by giving me enormous opportunities to interact and work with other laboratories. I would also like to express my gratitude to Professor Grodzinsky, my thesis committee, for the professional support and for teaching me lots of invaluable knowledge through the class.

I would like to thank all previous and current labmates at the d'Arbeloff lab and the labmates in Singapore for many helps and sharing all moments. I would like to express my sincere appreciation to Michaelle, Devin, Vincent, Mincheol, and Jacob, who especially helped me a lot as a member of the bio projects at MIT. I would also like to thank Tatsuya Osaki and members in the histology facility at the Koch Institute, including Charlene, Mike, and Kathy, for their generous support for my research and being a good friend with me. I would also like to thank all the MIT community, including all of staffs in the MIT facility and the MIT EHS, for providing me with a wonderful environment to research and helped me whenever I ask them for help.

I would like to thank the National Science Foundation (grant no. CBET-0939511), the Science and Technology Center for Emergent Behavior of Integrated Cellular Systems (EBICS), the Singapore-MIT Alliance of Research and Research Technology (SMART), and the Samsung Scholarship Foundation for their financial support.

Last but not least, I sincerely thank my family and close friends in the United States and Korea for sending me the unlimited and warm mental support from my side. Also, I am grateful to him for running a long course of marathon called the Ph.D. program with me and supporting me so that I could cross the finish line.

Contents

List of Figures

Chapter 1

Introduction

1.1 Motivation

Engineered skeletal muscle tissues (eSMTs) are three-dimensional (3D) tissues made from muscle cells and scaffolds in the laboratory. They require appropriate soluble factors and mechanical cues during the *in vitro* culture to recapitulate the function and structure of natural skeletal muscles. These eSMTs have a variety of applications in the medical and engineering fields, such as drug testing, implantation, and actuation of biological machines.

First of all, 3D eSMTs recapitulate the function and structure of natural muscles have been used in preclinical drug discovery [2] to reduce the costs of drug development and animal tests [3, 4]. In the preclinical testing for a drug, conventional 2D *in vitro* cell culture models poorly reproduce the physiological and pathological complexity of the human body, and the testing results from *in vivo* animal models show critical interspecies differences in disease mechanisms [4, 5, 6]. To overcome these problems, organs-on-a-chip (OOC) has been developed to mimic the microarchitecture, functions, heterotypic cell-cell interactions, and complex chemical and mechanical cues of real organs using human cells [4]. Since skeletal muscle comprises approximately 40% of the human body mass, the development of an in vitro skeletal muscle model is significant as part of the OOC [7].

Besides, eSMTs have been used as implantable tissues that improve muscle func-

tion in patients with volumetric muscle loss (VML), from which one cannot recover naturally [8, 9, 10]. In particular, when a large amount of muscle grafts is needed for implantation, such as VML, lack of implantable tissue or donor site morbidity can be severe problems. Also, implantation of the eSMTs using patient cells, such as human induced pluripotent stem cells or primary cells, can reduce the risk of immune rejection [11]. Moreover, eSMTs have been used as actuators for engineering biological machines, such as grasping or walking across a surface using a design strategy and coordinated muscle movements [12, 13, 14]. To utilize eSMTs practically, they should have a similar level of the functions and key features of natural muscles.

1.2 Literature review

To meet the numerous needs of eSMTs, 3D eSMTs have evolved to be more similar to natural skeletal muscles after they were first constructed by Strohman *et al.* in 1990 [15]. They developed a method to spontaneously form the 3D tissues through the detachment of myocytes and fibroblasts from a 2D synthetic membrane and rolling up after they were cultured about a week. This method was later refined by Dennis *et al.* [16] and they termed these 3D constructs as myooids. In 1991, Vandenburgh *et al.* created well-aligned 3D tissues, as natural skeletal muscles, by applying mechanical stretching from the monolayer of myoblasts on the stretchable membrane to the spontaneous formation of 3D tissue [17]. Lam *et al.* also obtained 3D muscle constructs with improved contractile forces using a micropatterned synthetic membrane through the alignment-mediated promotion of muscle differentiation [18].

Unlike the previously described 2D to 3D formations, Okano *et al.* successfully fabricated rod-shaped tissues by gelating the myoblast-embedded collagen I solution in a cylindrical mold [19]. This technique allows 3D eSMTs to be constructed in various shapes and sizes according to their mold including a ring shape [20, 21]. Instead of the natural hydrogel, synthetic biodegradable polymers such as poly-(L-lactic acid) and polylactic-glycolic acid were also used as a tissue scaffold [22, 23]. These 3D tissue formation methods using scaffolds aligned the muscle cells as well

by fixing both ends of the tissue with metal, velcro, or polydimethylsiloxane (PDMS) during cell-mediated gel compaction to produce axial stress [24, 25, 26].

Based on the previous work, our group developed a new method to form the 3D muscle tissues, called the fascicle-like 3D eSMTs [27]. This technique uses the gelatin sacrificial mold, which can shape the tissue like a natural fascicle and be easily removed after the tissue formation by medium change. In addition, both ends of the tissues are anchored to the PDMS to align the myotubes in the longitudinal direction of the tissues, and there is no hard contact with a hard surface except at the ends, to promote the better diffusion of the surrounding culture medium into the tissues. Moreover, the no hard contact in the middle allows the axial stress produced by the cell-mediated gel compaction to be uniform in the tissue. Furthermore, the fascicle-like eSMTs were fabricated by mixing myoblasts and the natural hydrogel scaffold, particularly fibrin and Matrigel, to have high volumetric cell density. Using these features of accessibility to the tissue, no hard contact, and the long rod shape like a fascicle, a novel force measurement system was developed to quantify the force generation, which is one of the basic functions of the skeletal muscle [1]. In these eSMTs, striated α-actinin, which is a marker of muscle contractility, and tetanus have been observed [27]. Because of these compelling advantages, this technique was used to fabricate and characterize eSMTs in this thesis.

1.3 Scope of the thesis

Although the formation of the fascicle-like eSMTs is an advanced tissue-engineering technique, there are still limitations in the previously developed eSMTs including the fascicle-like eSMTs to be widely utilized in the practical applications instead of natural skeletal muscles. Firstly, a contractile force of the current eSMTs is still in the range of 1 to 45 kPa [1, 28, 29, 30] although natural skeletal muscles generate approximately 250 kPa [31, 32]. Moreover, the size of eSMTs, which do not have any perfusable blood vessel to supply oxygen and nutrients and remove waste from host tissues, cannot be greater than the diffusion limit. Since their environments *in vitro* are much

simpler than the extremely complex one *in vivo*, which incorporates many types of cells, mechanical cues, and sophisticated microstructures, we hypothesized that these limitations are caused by missing key elements from natural skeletal muscles that are required to be stronger and bigger eSMTs. The inferior contractile performance and restricted size may decrease the predictability of drug-induced muscle response, delay functional recovery after implantation, and prevent the construction of large-sized eSMTs for treating the VML; thus they should be addressed appropriately for practical applications of eSMTs.

This thesis proposes two new approaches to improve the limitations in contractile force and size by applying the solutions of a *in vivo* system to *in vitro* eSMTs. Inspired by the fact that natural muscles are exposed to both electric potentials from motor neurons and mechanical stretching from surrounding muscles, a novel muscle training system using coordinated electrical and mechanical stimulation to improve the contractile force of eSMTs is described in chapter 2. In chapter 2, the increased contractile force by stimulation is explained in relation to changes in the extracellular matrix (ECM) network configuration. In chapter 3, *in vitro* vasculature was constructed in eSMT to increase the size of the tissue. Chapter 3 describes a newly developed coculture platform to vascularize eSMTs, which provides two separate culture media for each cell type to mimic the extracellular fluid compartments between blood plasma and interstitial fluid in the body. By using this innovative platform, the integrative effects of incorporating the perfusable vasculature through the eSMTs, the fluid compartments, and the temporal coordination of coculturing timing were investigated. Finally, the important findings of each chapter are summarized and directions of future work are discussed in chapter 4.

Chapter 2

Extracellular matrix remodeling induced by coordinated electrical and mechanical stimulation increases the contractile force

This chapter is modified from Ref. [33] with the publisher's permission.

2.1 Introduction

Engineered skeletal muscle tissue (eSMT) is made of myoblasts and extracellular matrix (ECM). To be contractile eSMT, myoblasts become myotubes through cell fusion, and then myotubes should be further matured through muscle differentiation. Muscle training is well known as a key step in myotube maturation to achieve a higher contractile force of eSMTs. Previously, electrical or mechanical stimulation has been applied for several days to weeks to obtain more proliferation and differentiation [34, 35, 36]. Although those training methods helped to increase the muscle performance, the trained eSMTs still displayed a significantly lower contractile force than natural muscles [37].

The limited performance of eSMTs is due to several differences between eSMTs

and native muscles, such as less differentiated myotubes, a low cell density, less organized sarcomeres and immature Ca^{2+} handling [38]. In particular, distinct features of the eSMT ECM significantly influence the force production and transmission. The ECM in natural skeletal muscles mainly comprises collagens [39, 40] and each myofiber is circumferentially surrounded by a 3 to 4.5 μm thick ECM layer, called the endomysium [41]. Active force is generated from sarcomeres in myofibers and transmitted to the ECM through costameres [42]. The ends of myofibers inside a fascicle are serially connected to other myofibers, mostly by overlapping with each other [39] or sometimes through very short collagen-bridged junctions that are less than 10 μm in length, termed intrafascicularly terminating ends [43, 44]. Unlike the natural skeletal muscle tissues, eSMTs currently have a higher volume fraction of the ECM gel. Moreover, eSMTs are usually formed by a mixture of myoblasts and the ECM and then cultured for up to 3 weeks. In the eSMTs, myoblasts fuse to form myotubes and premature myofibers during this period, but they are still thinner and much shorter with less muscle differentiation than natural adult muscles. Thus, the eSMTs have a thicker ECM layer, approximately 5 to 15 μm thickness, between myotubes. Additionally, a multitude of the shorter myotubes is connected serially at the intrafascicularly terminating ends, which are approximately 2 to 100 μm long, where the connecting ECM is much longer than in natural muscles (10 μm). Notably, these differences in the ECM significantly decrease muscle performance [31]. The much thicker ECM of the eSMTs impedes the muscle contraction by increasing stiffness of the ECM network and the nonfunctional fibrotic part [45]. Furthermore, the strength and stiffness of serial connections between the shorter myotubes are critical for the longitudinal transmission of tension. Therefore, the parallel ECM at the side of the myotubes must be soft, but the serially connected ECM at the intrafascicularly terminating ends must be stiff to transmit a higher force.

The ECM network is remodeled as it is exposed to mechanical stress and strain that change fiber orientations and their connectivity. Consequently, while most muscle training is designed to facilitate muscle differentiation, training of eSMTs may cause remodeling of the ECM fibers surrounding the myotubes as well as the ECM

connecting myotubes in series. Mechanical stretching generates tensile stress on the whole ECM in the direction of the load. In addition, muscle contraction triggered by an electric potential induces shear stress on the ECM at the side of the myotubes [39, 46] and tensile stress at the intrafascicularly terminating ends [47]. The application of these electrical and mechanical stimulations to the eSMTs may have a significant impact upon the remodeling of the ECM [48, 49].

Inspired by the fact that the regenerating parts of natural muscles are naturally exposed to electric potentials from motor neurons in combination with mechanical stretching from surrounding muscles, we hypothesize that applying a combined electrical and mechanical stimulation in a coordinated manner may produce higher contractile forces in eSMTs than a single type of stimulation. We aim to explain the increase in the contractile force in relation to changes in the ECM network configuration. It is known that mechanical changes in the viscoelastic eSMTs strongly depend on time [50]. Therefore, temporal coordination of electrical and mechanical stimulations is important to produce desired changes in the ECM. In this thesis, we show how the two types of stimulation should be combined and coordinated in a programmable manner with a certain phase shift and frequency.

Previously, several studies have applied static stretching with electrical stimulation to the natural skeletal muscles [51, 52, 53]. More studies on combining electrical and mechanical stimulations in a coordinated manner are needed to understand their synergistic effects on muscle training. Recently, in vitro systems for combined stimulation were developed for human mesenchymal stem cells [54], induced pluripotent stem cell-derived human cardiac tissue [55], rat cardiac cells [56], and mouse skeletal myoblasts [57], but no report has described temporal coordination, particularly the alternation of the two types of stimulation for eSMTs, instead of their synchronization. To our knowledge, this work is the first to assess the synergistic coordination of electrical and mechanical stimulation and utilizing it to enhance the contractile force of eSMTs by inducing structural remodeling of the ECM. We used fascicle-inspired three-dimensional (3D) eSMTs created with high-density and aligned C2C12s, mouse skeletal muscle myoblasts, and the fibrinogen/Matrigel ECM using a sacrificial mold-

ing technique [1] (Fig. 2-1). Several unique features of these eSMTs made them suitable for use in this study. The fascicle-inspired eSMTs only contact a culture medium, without any hard contact except for both ends; this design allows the tissue to have uniform axial stress during an external mechanical stretching and less hindrance to muscle contraction during an electrical stimulation. In addition, a system for measuring the contractile force of the fascicle-inspired eSMTs was developed [1]. We applied the external stimulation to the eSMTs for only 3 minutes to focus on the changes in mechanical properties and reduce possible effects caused by changes at the RNA/protein levels [58], such as proliferation and differentiation. We built a mechanistic model to better elucidate the effect of ECM remodeling upon the generation and transmission of the eSMT contractile force.

2.2 Materials and methods

2.2.1 Cell culture

The C2C12 mouse myoblast cell line (ATCC, Manassas, VA, USA) was used for the experiments in this chapter. Myoblasts were maintained in the growth medium (GM) comprising Dulbecco's modified eagle medium (DMEM, Sigma-Aldrich, St. Louis, MO, USA) supplemented with 10% fetal bovine serum (FBS, Sigma-Aldrich, St. Louis, MO, USA), 1% penicillin-streptomycin (PS, Sigma-Aldrich, St. Louis, MO, USA), and 0.2% Normocin (InvivoGen, San Diego, CA, USA). Cells were passaged when they reached 70% confluence to ensure that the cells remained unfused. The growth media was changed daily after we seeded the cells in the fabricated chip to form the fascicle-like eSMTs.

2.2.2 Fascicle-like eSMTs

The 3D fascicle-like muscle constructs used in this thesis were formed using the sacrificial molding technique [27]. The eSMT made using this new technique is a 6 mm long and about 0.1 mm thick well-aligned tissue in 3D environment. This special tissue is

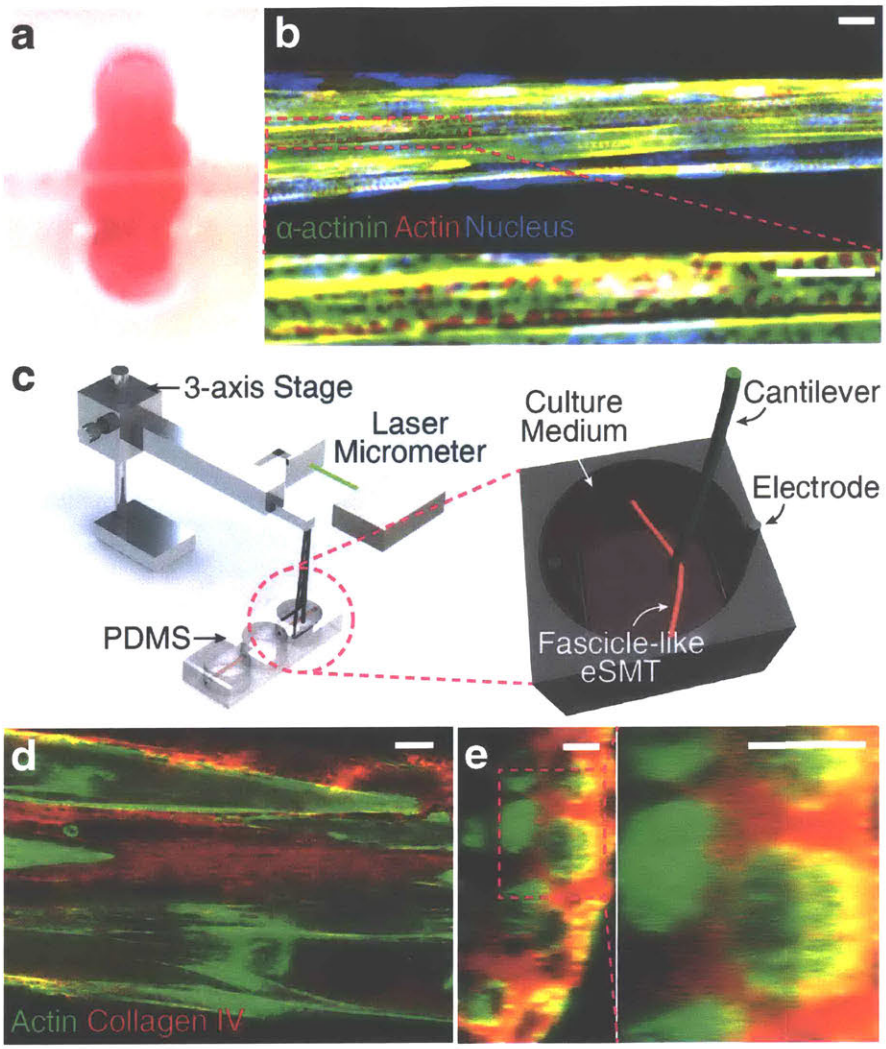

Figure 2-1: Co-stimulation system and fascicle-like engineered skeletal muscle tissue (eSMT). **a**, **b**. The fascicle-like eSMT formed a cylindrical shape with length of 6 mm and diameter of approximately 75 μm (**a**). The tissues were stained using immunofluorescence technique to visualize the striations of α-actinin, which is a marker of differentiation and contractility (**b**, Reproduced from reference [1] with permission from the Mary Ann Liebert, Inc., New Rochelle, NY). Scale bars represent 5 mm in (a) and 10 μm in (b). **c**. Schematic of the experimental setup used to apply coordinated electric and mechanical stimulation to the eSMT. The co-stimulation system consists of electrodes for applying the electric potential, a cantilever wire moved by a servomotor, and a laser micrometer to monitor the displacement of the cantilever. The eSMT is pulled sideways with the cantilever to stretch eSMT to the desired strain. Contractile force was quantified by measuring deformation of the cantilever whose bending stiffness is known. **d**, **e**. Cross-sectional images of unstimulated eSMTs stained for collagen IV (red) and actin (green) in longitudinal (**d**) and transverse (**e**) directions. Scale bars represent 10 μm.

only anchored at both ends, and there is no hard contact in the middle of the tissue. Therefore, this enables improved diffusion of medium into the eSMT, and the whole tissue has the uniform tensile stress by cell-mediated gel compaction. There were multiple steps to make the fascicle-like eSMT. Steel pin with nominal diameter 508 μm was inserted into the mold that was printed using 3D printer (Dimension 1200es, Stratasys, Eden Prairie, MN, USA). After poured Polydimethylsiloxane (PDMS) was solidified in the mold, removing the steel pins made the tubular holes in the PDMS. 6 mm holes were formed using a punch. The size of the holes decides the length of the muscle tissue and the holes were used as a reservoir for medium. The PDMS chips were cut into small pieces with 3 holes each and bonded with 0.5 mm thin PDMS film. Before putting the cells into the fabricated chips, the chips were autoclaved in order to prevent contamination. One of the key techniques for the fascicle-like device was the sacrificial molding to make tubular shape of the eSMT. The material for the sacrificial mold should be kept solid at blow a certain temperature and form desired shape. However, it should be melted at high temperature to remove the sacrificial mold. Thus, we used 5% gelatin solution melted at 37 °C to growth medium and solidified at room temperature The gelatin solution also contained thrombin to use fibrin as the ECM, and 0.05 M NaOH solution for pH adjustment. This gelatin solution was poured into the PDMS chips with a pin, and the chips were in the refrigerator for 30 minutes to accelerate gelatin solidification. The trypsinized C2C12 mouse myoblasts were centrifuged, and the cell pellets were mixed with 80% fibrinogen (Sigma-Aldrich, St. Louis, MO, USA), 20% growth factor reduced Matrigel (Corning, NY, USA), and cold growth medium (DMEM, Sigma-Aldrich, St. Louis, MO, USA). After removing the pins from the gelatin-solidified chips, the cell and gel mixture was injected in the holes of the gelatin sacrificial mold. In the 37 °C incubator, gelatin-thrombin solution was melted and formed the fibrin matrix. Remaining gelatin was diluted out through medium change every day. For two days after seeding, the cells were cultured in GM with 1 mg/mL aminocaproic acid (AA, Sigma-Aldrich, St. Louis, MO, USA). AA was added to mitigate ECM degradation. After that, we changed the media into muscle differentiation medium (MDM) with 1 mg/mL AA to induce muscle cell development

in vitro. MDM was the same as GM except for 4% horse serum instead of the fetal bovine serum (FBS). The medium was changed every day for totally 10 days.

2.2.3 Measurement of the contractile forces of skeletal muscles

Using the single apparatus, we not only applied the co-stimulation to the eSMT, but also measured its contractile force. Unlike the isometric force measurements in previous researches inhibits shortening of muscle tissues, we measured the concentric contractile force with shortening, which is a more natural way to contract. To allow muscle to shorten during contraction, first we stretched muscle (2.3% strain) using the tip of the cantilever wire (Enameled Copper 33 AWG, Remington Industries, Johnsburg, IL, USA). Then, a tension of the stretched eSMT and a restoring force of elastic wire were balanced (Fig. A-1). When we apply the electric potential (1.5 V/mm, bipolar pulses of 1 ms each, for 3 seconds) additionally, the wire tip is displaced because of the additional contractile force towards muscle's original position during the shortening (Fig. A-1). We use the same cantilever wire for all the results here, thus the stiffness of the tip kept the same value. We track the displacement of the wire tip using the tracker program (comPADRE). In Fig. A-1, yellow dot is the original force equilibrium position, and the dot is shifted to the red dot by the contractile force. The distance between the two dots is proportional to muscle contractile force.

2.2.4 Co-stimulation system

A programmable co-stimulation system was constructed by integrating an electric device required to generate an electric potential and a motor-driven stage (Thorlabs, Auburn, CA, USA) for stretching 3D eSMTs, both of which were controlled by a computer (Fig. 2-1c). The electric potential was administered with two platinum wires placed in the medium beside the muscle tissue using a 3D printed wire holder (Dimension 1200es, Stratasys, Eden Prairie, MN, USA). An electrical field of 2.5 V/mm was applied with bipolar pulses of 1 ms each for 0.5 seconds per time for

training. The two electrodes were placed parallel to the longitudinal direction of the eSMT, and the electric field was generated between the electrodes perpendicular to their direction. Mechanical stretching was produced through the cantilever wire (Enameled Copper 33 AWG, Remington Industries, Johnsburg, IL, USA) by pulling the muscle sideways (Fig. A-1).

2.2.5 Immunostaining

Type IV collagen was immunostained with primary antibodies against collagen IV (Sigma-Aldrich, St. Louis, MO, USA) and α-actinin (Thermo Fisher Scientific, Waltham, MA, USA) after fixing the trained eSMTs with 4% paraformaldehyde (Santa Cruz Biotechnology, Dallas, TX, USA), and permeabilizing them with 0.2% Triton-X (Thermo Fisher Scientific, Waltham, MA, USA). Trained eSMTs were incubated with 1% bovine serum albumin (Sigma-Aldrich, St. Louis, MO, USA) to block the nonspecific binding of antibodies. Hoechst (Thermo Fisher Scientific, Waltham, MA, USA) and rhodamine phalloidin (Thermo Fisher Scientific, Waltham, MA, USA) were applied together for 30 minutes to visualize nucleus and actin, respectively.

2.2.6 Measurement of the orientation distribution of ECM fibers and sarcomere length

We used the ImageJ plugin OrientationJ [59] and DDecon (The Scripps Research Institute, La Jolla, CA) to measure the orientation distributions of the collagen IV fibers and sarcomere length in the immunostaining images, respectively.

2.2.7 Statistical analyses

Statistical analyses were conducted using Student's t-test. Data were considered statistically significant if the P-value was 0.05 (*), 0.01 (**), or 0.001 (***).

2.3 Results

2.3.1 Increased contractile forces generated through short-term training with diverse types of stimulation

We developed a testbed that applies combined electrical and mechanical stimulation, which is defined as co-stimulation. Fascicle-like eSMTs with pronounced α-actinin striation were formed using a 3D sacrificial molding technique and suspended between two holes (Fig. 2-1a-b). We modified an existing system [1] into a new testbed that allowed us to apply mechanical stretching and electric potential, as well as to facilitate contractile force measurements (Fig. 2-1c and A-1). We used a cantilever wire with a known stiffness to measure contractile force and to stretch the eSMT by pulling it in the direction perpendicular to the longitudinal direction of the eSMT. The cantilever was moved by an actuator that was programmed to stretch tissue to the desired strain. We also simultaneously administered an electric potential using the platinum electrodes to achieve combined electrical and mechanical stimulation.

Both electric potential and mechanical stretching were repeatedly applied to the eSMTs (Fig. 2-2a). The two periodic stimulations were alternated with phase differences of 0°, 90°, 180°, and 270°. Although an electromechanical coupling of contraction exists [60, 61], the delay time of the coupling is only 30 to 100 ms [60], which is almost negligible compared to one period of the stimulation used in this study (4.3 s). The contractile force of the trained eSMTs was normalized by the original contractile force before the training to evaluate the performance improvement. Interestingly, a 180° of phase shift produced the greatest performance improvement and achieved nearly 20% better performance than the 270° phase shift (Fig. 2-2b), although all other conditions were identical. Furthermore, we applied the co-stimulation at diverse frequencies in similar range reported in previous studies, spanning 0.1-0.5 Hz [62, 63, 64]. When we applied the co-stimulations at three frequencies of 0.1, 0.23, and 0.45 Hz, the contractile force was more improved to a greater extent when stimulated at 0.23 Hz (Fig. 2-2c). In addition, the out-of-phase (180° phase shift) co-stimulation

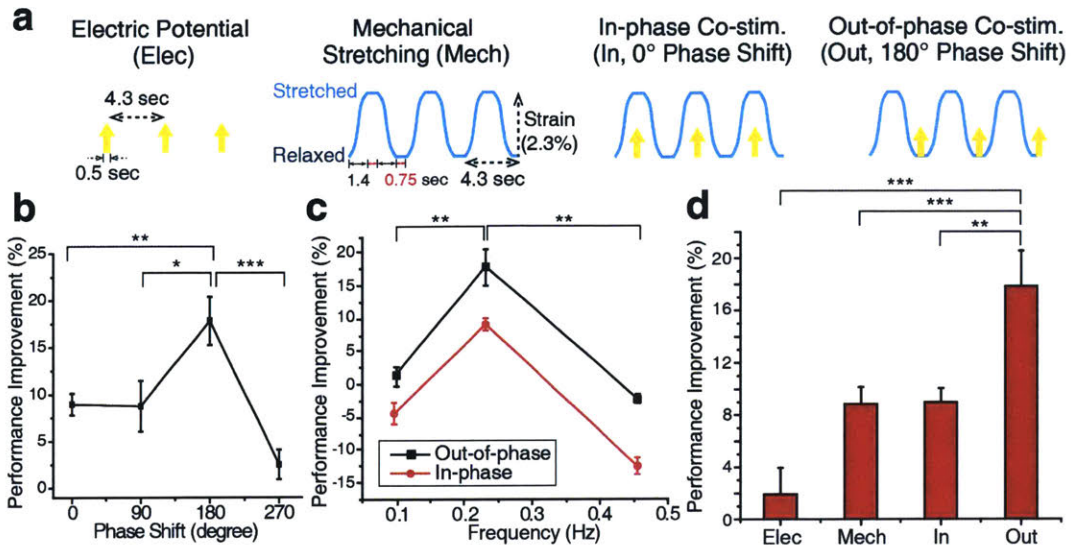

Figure 2-2: Coordination of the combined electric and mechanical stimulation and synergistic performance enhancement following 3 minutes of stimulation. **a**. Four patterns of coordination: electrical (Elec) and mechanical (Mech) stimulations alone, and in-phase (In, 0° phase shift) and out-of-phase (Out, 180° phase shift) co-stimulations. **b**. Improvement in the contractile force induced by the combined stimulation with different phase shifts. SEM, $n = 10, 5, 10$, and 5. **c**. Improvement in the contractile force induced by stimulations with different frequencies. SEM, $n = 3, 10$, and 3. **d**. Comparison of the performance improvements in the contractile force induced by the four patterns of stimulation in (**a**): the two single types of stimulation (Elec and Mech) and two co-stimulations (In and Out). SEM, $n = 9, 11, 10$, and 10. Out-of-phase co-stimulation increased the contractile force by 18% in 3 minutes. $^{*}P < 0.05$, $^{**}P < 0.01$, and $^{***}P < 0.001$.

improved the performance more than the in-phase (0° phase shift) co-stimulation, regardless of frequencies (Fig. 2-2c). Therefore, we chose the out-of-phase co-stimulation at 0.23 Hz as the condition to effectively enhance the contractile force.

Co-stimulation was also compared to individual electrical (Elec) and mechanical (Mech) stimulations (Fig. 2-2d). The average contractile force of the eSMTs before the stimulation was 4.0 ± 1.7 μN. The performance improvements of single stimulation types were significantly inferior to the out-of-phase co-stimulation (Out), which produced an 18% of improvement after only 3 minutes of training (Fig. 2-2d). A synergistic improvement was observed in the out-of-phase co-stimulation, compared to the single type of stimulation. The in-phase co-stimulation (In), on the other

hand, yielded only an 8.9% improvement, a value that was less than the out-of-phase condition and similar to the mechanical stimulation alone.

2.3.2 Mechanistic model of a myotube in the eSMT coupled with the surrounding ECM

In an attempt to elucidate the cause of the significant increase in contractile force induced by short-term training, a simple mechanistic model for the myotube in the eSMT was constructed. In the experiments described above, a significant increase in force was obtained in only 3 minutes of the training. This implies that mechanical factors may be responsible for the improvements rather than biochemical factors, which would need more time to cause such significant changes. Myotubes are extensively coupled with the surrounding ECM and, thereby, the net contractile force of the eSMT is highly dependent on the ECM properties. Mechanical factors of the muscle tissues are attributed to active and passive elements (Fig. 2-3a). Sarcomeres inside the myotube, which generate contractile force, represent the active element (AE). The passive elements (PE) comprise all the components that do not produce a force in the tissue, including the ECM and non-contractile parts of muscle cells. However, a noticeable difference between the actin networks in the eSMTs was not observed following the administration of the difference stimulations for 3 minutes (Fig. A-2), as all of the actin fibers were well-aligned in the longitudinal direction.

As we mentioned above, the ECM of the eSMTs shows distinct features from the ECM of natural skeletal muscles: a) much thicker ECM layers in parallel to the myotubes, and b) a much longer serial ECM that connects the two ends of the intrafascicularly terminating myotubes (Fig. 2-1d-e). These coupled myotubes and ECM properties were represented with a mechanistic model consisting of the parallel and serial passive elements (Parallel PE and Serial PE, respectively) in conjunction with the AE (Fig. 2-3a). According to this model, as the stiffness of the Parallel PE increases, the displacement induced by the contractile force at the AE decreases. This explains possible impediments of muscle contraction due to the thick ECM,

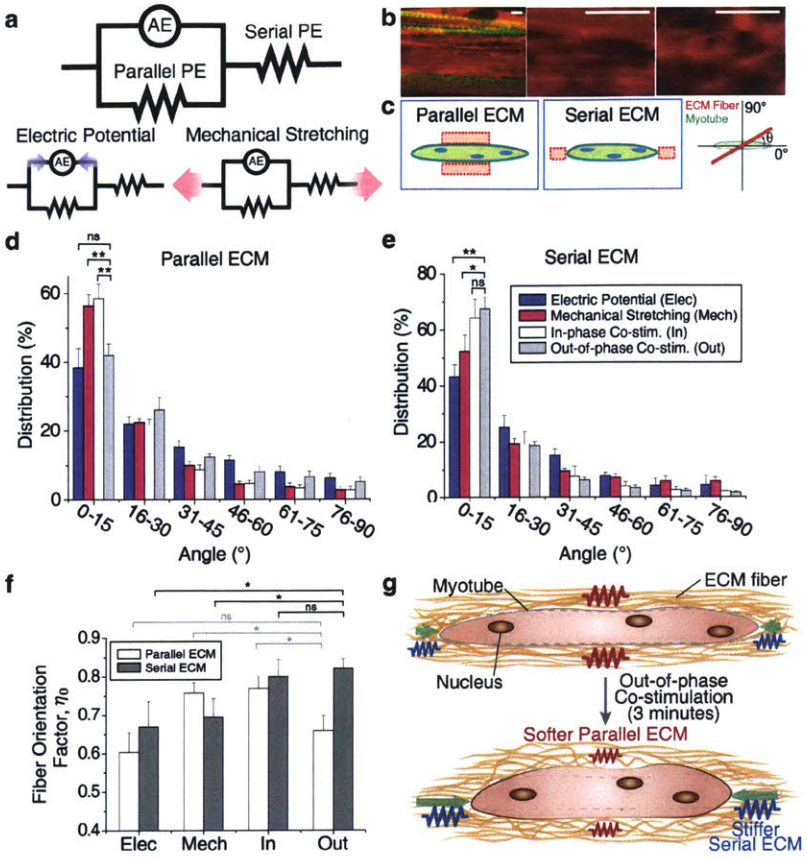

Figure 2-3: Mechanistic model of eSMT force generation and transmission, and changes in the mechanical property induced by ECM remodeling. **a**. Mechanistic model of eSMT consisting of an active element (AE), parallel passive element (Parallel PE), and serial passive element (Serial PE). **b**. Images of collagen IV (red) and actin staining in the myotubes (green) of the eSMTs to measure the fiber orientation distribution of the ECM network (left). Images of well-aligned collagen fibers (middle) and less-aligned fibers (right). Scale bars represent 5 μm. **c**. Schematics showing the regions of the parallel and serial ECMs relative to the myotubes, and ECM fiber orientation θ measured from the longitudinal direction of myotube. **d**, **e**. Orientation distribution of collagen IV in the parallel (**d**) and serial (**e**) ECM regions. Most ECM fibers were aligned parallel to the longitudinal direction of the myotubes (0°) by pretension. SEM, $n = 8, 12, 11$, and 10 (parallel), $n = 3, 7, 3$, and 7 (serial). **f**. Comparison of fiber orientation factors (η_o) to predict the elastic modulus of the ECM network (E_L). The out-of-phase co-stimulation induced the highest elastic modulus (largest η_o) for the Serial PE and a low elastic modulus for the Parallel PE. SEM, n is the same as **d** and **e**. $^*P < 0.05$, $^{**}P < 0.01$, and ns, not significant. **g**. Schematic depicting the mechanism underlying the changes in performance induced by ECM remodeling following the application of the out-of-phase co-stimulation. The out-of-phase co-stimulation decreases the stiffness of the parallel ECM for less impedance on muscle contraction and increases the stiffness of the serial ECM to increase force transmission to the load.

particularly when the ECM is stiffer than myotubes [65]. The mechanistic model also explains that the force generated from the active element cannot be transmitted to the load when the Serial PE is too soft. Therefore, the contractile force generated from the myotubes of the eSMTs is not transmitted well to the end of the tissue if they are connected by a soft serial ECM. In summary, the parallel ECM should be soft, but the serial ECM should be stiff enough to transmit a higher contractile force.

2.3.3 ECM fiber orientation

Based on the mechanistic model that shows the mechanical effects of the Parallel and Serial PEs on the force generation, we hypothesized that effective structural remodeling of the parallel and serial ECMs is induced by the out-of-phase co-stimulation compared to other training methods (Fig. 2-2d). We assumed that 3 minutes of the training did not change the composition and amount of the ECM because the time was too short to produce significant quantities of new ECM proteins. We measured the distribution of the ECM fiber orientations of the trained eSMTs to examine the changes in the mechanical property of the ECM network. The endomysium of the natural muscles contains collagen I, III, IV, and VI [66, 67]. Collagen IV, which is one of the main components of the muscle ECM, particularly in the ECM surrounding newly formed myotubes during skeletal muscle regeneration [68], contributes to muscle contraction by attaching to a sarcolemma and connecting the other types of collagen to myotubes [67, 69]. In this sense, collagen IV and muscle contraction are significantly influenced by each other through the cell-ECM interaction. In the case of the eSMTs, myoblasts were seeded with a fibrin and the Matrigel matrix to form the tissue. Staining of collagen IV, which is one of the main components of the Matrigel, showed that myotubes were largely surrounded by collagen IV (Fig. 2-1e). When we imaged fibrin, the training did not produce any noticeable change in fibrin, which consists of a highly aggregated network (Fig. A-3). Therefore, we observed collagen IV near the myotubes to study the effects of the structural remodeling of the ECM induced by the stimulation on the contractile performance.

After we trained the eSMTs with the four different methods shown in Fig. 2-2d,

the collagen IV network of the eSMTs was imaged (Fig. 2-3b) to measure the fiber orientation distributions at the parallel and serial ECM regions (Fig. 2-3c). The orientations of the fibers were mostly aligned in the longitudinal direction of the myotubes (0°) due to the pretension generated during the formation of the fascicle-like eSMTs (Fig. 2-3d-e). From the orientation distributions, we compared the elastic modulus of the ECM network (E_L) in the longitudinal direction to the myotubes using the rule of mixtures: $E_L = \eta_o E_f V_f + E_m V_m$, where η_o is fiber orientation factor, E_f is the elastic modulus of the single ECM fiber, E_m is the elastic modulus of medium, V_f is the volume fraction of the ECM fiber, and V_m is the volume fraction of medium [70]. We set θ to the angle of the ECM fiber with respect to the longitudinal direction of the myotubes (Fig. 2-3c) and $f(\theta)$ to the proportion of fiber content in the angle θ. The fiber orientation factor was calculated as $\eta_o = \int f(\theta) \cos^4 \theta d\theta$. The value of this equation becomes 1 when all the fibers in the network are aligned in the loading direction (0°) and 0.375 for randomly oriented fibers. We assumed that 3 minutes of the training did not influence E_f or V_f, and thus the dominant change caused by the training was the fiber orientation. Since E_m for the liquid medium in the network is almost zero, the $E_m V_m$ term is negligible. Therefore, we compared E_L of the parallel and serial ECM regions in the trained eSMTs by calculating the fiber orientation factor η_o (Fig. 2-3f).

2.3.4 Changes in ECM fiber orientation of the eSMTs upon stimulation

Differences in the distributions of fiber orientations shown in Fig. 2-3d-e indicate that each type of stimulation exerted a different effect on the structural remodeling of the ECM. As summarized in Fig. 2-3f, the out-of-phase co-stimulation generated the highest fiber orientation factor for the collagen IV network of the serial ECM and the low orientation factor for the parallel ECM. Therefore, the out-of-phase co-stimulation induced the greatest stiffness in the serial ECM and a low stiffness for the parallel ECM, both of which are desired for effectively generating and transmitting

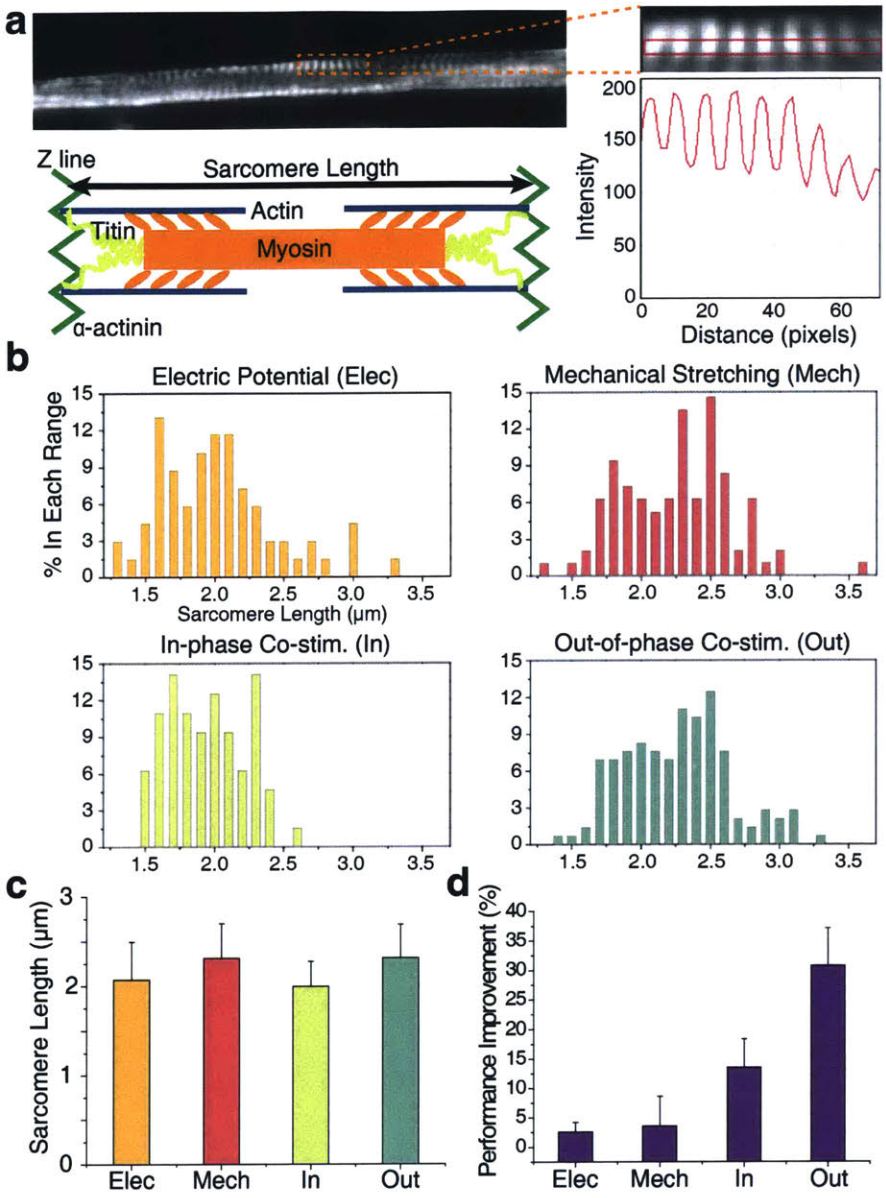

Figure 2-4: Investigation of changes in the active element and long-term (20 minutes) effects of the stimulation. **a**. Measurement of sarcomere length based on the intensity of α-actinin immunostaining images. The schematic shows the sarcomere structure and length. **b**. Percentages (%) distributions of sarcomere length in each range after applying the electric potential (Elec), mechanical stretching (Mech), in-phase co-stimulation (In), and out-of-phase co-stimulation (Out) for 3 minutes. **c**. Average sarcomere length after applying the four different types of stimulations: Elec, Mech, In, and Out. SD, $n = 69, 96, 64$, and 145. **d**. Longer-term performance enhancement of the eSMTs' contractile force following the application of the four stimulations for 20 minutes, SEM, $n = 3$ for all. Out-of-phase co-stimulation enhanced the contractile force by 31% in 20 minutes.

a contractile force (Fig. 2-3g). According to Fig. 2-3e, the electrical stimulation alone did not adequately align the fibers of the serial ECM. On the other hand, the mechanical stimulation alone resulted in more aligned fibers of the serial ECM, but the alignment was less than that induced by the co-stimulations. In addition, the mechanical stimulation increased the alignment in the parallel ECM (Fig. 2-3d), which is not desirable. The in-phase co-stimulation also aligned more fibers of the parallel ECM than other stimulations. Therefore, as shown in Fig. 2-3, the out-of-phase co-stimulation most effectively increased performance by promoting the desired structural remodeling of the ECM, particularly by differently altering the ECM depending on its location relative to the myotube. Furthermore, these ECM remodeling improved both the contractile force and stability of the contractile force by switching from the unfused tetanus to fused tetanus (Fig. A-4).

2.3.5 Effect of the short-term stimulation on the active element

In addition to the changes in the passive elements, the active element might also contribute to the improvements in the force generated by the eSMTs (Fig. 2-3a). A sarcomere has an optimal range of lengths to produce a high active tension with optimal actin-myosin overlap, that is, 2 to 2.4 μm [71]. Therefore, we measured the sarcomere length in the trained tissues (Fig. 2-4a) to investigate the changes in the active element. Since the sarcomere length is the distance between adjacent Z-lines, we stained α-actinin of the trained eSMTs, a key component of the Z-line (Fig. 2-4a). The average sarcomere lengths after applying the mechanical stimulation and out-of-phase co-stimulation were 2.3 μm, and the lengths after applying the electrical stimulation and in-phase co-stimulation were 2.1 and 2.0 μm, respectively (Fig. 2-4b-c). Because all the lengths were ranged from 2 to 2.4 μm, the differences in the force generation due to the active element following the four different types of stimulations (Fig. 2-2d) were negligible. Consequently, the performance enhancement induced by the short-term stimulation resulted mostly from changes in the passive elements,

specifically through the ECM remodeling.

The four types of stimulations were administered for 20 minutes to examine the effects of longer stimulations. We obtained a 31% performance improvement in the contractile force for the out-of-phase co-stimulation (Fig. 2-4d), a value that was 1.7 times higher than the improvement induced by the 3-minute stimulation. Applying the co-stimulation for 20 minutes may induce more remarkable ECM remodeling than the 3-minute stimulation. This structural change in the ECM, which alters its mechanical properties, may affect muscle differentiation induced by mechanotransduction on much longer time scale than 20 minutes, as substrate stiffness has been shown to play an important role in muscle differentiation [72].

2.4 Discussions and future directions

Fascicle-like eSMTs improved the generation of contractile forces by 18% in 3 minutes and 31% in 20 minutes following alternating the two types of stimulation, electric potential and mechanical stretching. In contrast, the single type of stimulations produced significantly lower improvements: only 2% for the electric potential alone and 8.8% for mechanical stretching alone after 3 minutes of the stimulation. The sum of these two numbers is only 10.8%, which is approximately half of the increase in performance induced by the out-of-phase co-stimulation. Thus, alternating the two types of stimulation produces a synergistic effect. In addition, applying the in-phase and out-of-phase co-stimulations resulted in differences in ECM remodeling at the eSMTs, although they were subjected to identical electrical and mechanical stimulations.

Mechanical stretching applies a tensile stress to the eSMT, while electric potential causes contraction, which induces shear and compressive stresses. In the co-stimulation, where the two single stimulations are combined, temporal coordination of the various stresses is important to induce the appropriate ECM remodeling. In particular, in the parallel ECM, which should be less aligned in the myotube direction not to hinder the muscle contraction, the in-phase co-stimulation develops

both the shear stress and tensile stress simultaneously, which can create the highest shear stress, resulting in the highest parallel ECM alignment (the highest percentage of fiber distribution between 0 and 15 degrees). On the other hand, in the out-of-phase condition, this alignment is avoided by alternately administrating the two single stimulations. This difference leads to more ECM alignment of the parallel ECM in the myotube direction by the in-phase co-stimulation than the out-of-phase co-stimulation (Fig. 2-3d). In addition, the two co-stimulations further align the serial ECM to a greater extent (Fig. 2-3e) than the single stimulations (electric potential and mechanical stretching). This finding might be explained by the bi-polar, push-pull effects of alternating these two single stimulations on the ECM network, which can yield a grater ECM alignment than mono-polar effects induced by the single stimulations. Moreover, the ECM is a viscoelastic material with the characteristics of strain stiffening and stress relaxation. These properties will behave differently during the application of the two co-stimulations, which have different temporal coordination of the various stresses and result in the different ECM remodeling.

Although the out-of-phase co-stimulation produces more desirable ECM remodeling than the other stimulations, the difference between eSMTs and the natural skeletal muscles is still significant. The endomysium of natural muscles comprises a quasi-random network of wavy ECM fibers [39]. The ECM of the eSMTs was mostly aligned in the longitudinal direction to myotubes (Fig. 2-3d-e), because of a pretension between the fixed ends of the eSMTs generated by cell-mediated gel compaction. This ECM orientation was similar to the one of highly extended natural muscles [49]. In addition, the serially connected ECM at the intrafascicularly terminating myotubes should be stiff in the eSMTs for force transmission, but this is not required for the case of the natural muscles with myotubes of a sufficient length, which allows having myotube overlapping. In some regions, the serial ECM was also the parallel ECM for other myotubes. In this case, the ECM might be neither too stiff nor too soft to generate the force from the tissues. Moreover, the incorporation of fibroblasts, the major source of the endomysium, and the endomysium-embedded blood vessels into the eSMT will help to more closely mimic the mechanical and chemical environment

of the endomysium in native muscles. We also used the myoblast cell line (C2C12) to prepare the eSMTs that have been used in this chapter. If primary myoblasts were used, the eSMTs would have greater heterogeneity owing to donors variability, a lower myotube fusion rate because of a hindrance by non-myoblasts cells in cell population, and the ECM with distinct thickness and composition due to the influence of the non-myoblast cells. On the other hand, performing experiments with primary cells would allow us to study donor characteristics and mimic the tissue complexity caused by various types of cells. Therefore, future studies using primary cells would contribute to creating a personalized drug testing platform and understanding the diversity of native muscles.

An improvement in performance was obtained in only 3 minutes, but further investigations are needed to identify other possible mechanisms in addition to ECM remodeling. During such a limited time of 3 minutes, many mechanical and biological factors could be altered by the external stimulations, such as the production of reactive oxygen species (ROS) [73], opening of the stretch-activated channels (SACs), and cell fluidization [74]. However, changes in the ROS levels and opening of the SAC do not substantially affect the muscle contractile force in such a short time [75, 76]. Cell fluidization is characterized by an immediate reduction in F-actin levels right after stretching of the cells, but the F-actin levels are recovered completely within 5 minutes [74]. On the other hand, our results show that the improvement in the contractile performance of the trained eSMTs maintained for 3 hours ($-0.269 \pm 4.25\%$ change, $n = 4$). Applying a mechanical or electrical stimulation can also activate some translation/transcription-related mechanisms, such as PI3K/Akt/TOR signaling [77] and nitric oxide-activated proliferation [78]. However, transcription and translation speeds [79] are too slow to facilitate performance improvement in the stimulation time of 3 minutes. Therefore, we conjecture that the increase in contractile force of the eSMTs observed in a short time is likely due to the ECM remodeling rather than these biological changes. Even so, further investigation is required of other possible mechanisms that are potentially activated by the short-term stimulations.

In this thesis, we proposed a new method for increasing the contractile force of

the eSMTs through short-term stimulation. Alternating mechanical and electrical stimulations resulted in approximately a 18% higher contractile force in 3 minutes when the two stimulations are alternated with a 180° phase shift at a frequency of 0.23 Hz. In an attempt to explain the mechanism underlying the synergistic improvements induced by the co-stimulation, we generated a mechanistic model based on the morphology of the myotubes and the surrounding ECM in the eSMTs. We examined changes in both passive and active elements involved in the mechanistic model by measuring the orientation distribution of ECM fibers and the length of sarcomeres after applying the stimulation. This model and the experimental results showed how the out-of-phase co-stimulation mechanically enhanced the contractile force by inducing desirable ECM remodeling and cell-ECM interactions for force generation. We obtained two insights from these results: 1) coordinating and harmonizing the two stimulations that produce bi-polar effects is important to produce a higher contractile force of engineered muscles; and 2) the contractile force of engineered muscles is significantly improved not only by biological changes, such as differentiation and proliferation but also by mechanical changes. This work will contribute to overcoming the performance limitation of the engineered muscles and meeting the requirements for eSMTs to serve as a drug testing platform and actuators of micro bio-bots.

Chapter 3

Coaxial engineered human skeletal muscle tissue with tubular vasculature recapitulating the extracellular fluid compartments

3.1 Introduction

Various types of small engineered human skeletal muscle tissues (ehSMTs) and skeletal-muscle-on-a-chip have been developed to examine the dose-dependent recocse to myotoxic drugs [2], to study the physiology of human skeletal muscles [80], and for use as regeneration models [30]. Furthermore, it has been attempted to implant large ehSMTs for the treatment of volumetric muscle loss (VML) [81]. Implantation of ehSMTs composed of cultured muscle cells alleviates issues associated with donor site morbidity and the shortage of donor tissues [82]. However, the creation of the scalable ehSMTs, especially those over 200 μm in general and up to 1.5 mm in the case of *in vitro* skeletal muscle tissues [83], has been hampered by the problem of oxygen and nutrient diffusion, which induces hypoxia-induced necrosis and apoptosis [84, 85].

Vascularization is a critical requirement for many of these applications. In par-

ticular, prevascularization, defined as the creation of vasculature in tissue before implantation [86], is known to increase the viability of the implanted cells and promote recovery of the implanted site by facilitating connection to the host vasculature [87]. Furthermore, the prevascularization of ehSMTs can create the heterotypic cell-cell interactions between skeletal muscles and blood vessels *in vitro*, which affect their functionalities. Coculturing muscle cells with endothelial cells enhances myogenesis and muscle contractile performance through Angiopoietin-1/Neuregulin-1 signaling [88]. Conversely, angiopoietin-1 secreted by skeletal muscle myoblasts increases the angiogenic properties of endothelial cells [88, 89]. In summary, the formation of prevascularized skeletal muscle tissues is required to 1) scale up the ehSMTs beyond a diffusion limit, 2) increase the survival rate of implanted tissues, 3) better understand the physiological heterotypic cell-cell interactions, and 4) improve the functionalities of both muscle and endothelial cells in the ehSMTs.

Although culturing endothelial and muscle cells together is mutually beneficial, these cell types require different biochemical environments. It has been a challenge in *in vitro* cocultures to accommodate conflicting media requirements and provide both types of cells with desired microenvironments. To promote the differentiation of skeletal muscle cells *in vitro*, myoblasts need a muscle differentiation medium (MDM) containing low levels (2%) of horse serum (HS) and high levels (4500 mg/L) of glucose [90]. The low HS condition inhibits the proliferation of myoblasts and initiates the muscle differentiation with cell fusion. On the other hand, the endothelial cell growth medium (EGM) usually contains more nutrients than the MDM, supplemented with fetal bovine serum (FBS), vascular endothelial growth factor (VEGF), or bovine brain extract (BBE) to support endothelial cell growth. Additionally, since the compositions of sera, such as growth factors and immunoglobulins, notably vary with species and age [91], the use of the HS or FBS can affect the morphology and behaviors of the cells [92]. As a result, culturing myoblasts in the EGM (endothelial cell growth medium, EGM-plus, Lonza) yields much inferior contractile performance, and incubation of endothelial cells in MDM incurs apoptotic morphology (Fig. B-1 **a**,**b**). Desired nutrient conditions for the differentiation of skeletal muscle and growth of endothelial

cells are therefore conflicting. The current practice, however, mixes endothelial cells and muscle cells homogeneously and incubates them in a coculture medium (COM), usually a half-and-half mixture of the two media or containing many nutrients, which hinders the muscle differentiation [22, 93, 94]. Since merely using the mixed media cannot meet the requirement for both cell types at the same time, we hypothesize that coculturing the two cell types with two separate media enhances muscle differentiation and blood vessel formation compared to coculturing with the mixed media.

In the body, different extracellular fluids are compartmentalized between blood plasma in the capillaries and interstitial fluids in skeletal muscle tissues [95] (Fig. 3-1**a**). Here, we aim to model these fluid compartments for ehSMTs to solve the incompatible medium problem and investigate the effects of coculturing endothelial cells and skeletal myoblasts. To closely mimic the fluid compartments *in vivo*, three functional requirements must be considered. One is that the two media must be separated through a perfusable vascular channel. Second, the same type of cells must be lumped together, rather than mixing one type with the other, so that each cell cluster can be exposed to a separate chemical environment. For myoblasts, lumping the cells of the same type also promotes cell fusion to create myotubes since the fusion needs direct contact between adjacent myoblasts. Third, the two types of cells must be placed proximately enough to interact through paracrine signaling. A new approach to forming vascularized ehSMTs is required to meet these requirements.

Previous studies on the vascularization of ehSMTs have used a single mixed coculture medium. Vascular networks have been formed in the engineered skeletal muscles [94, 96], but they are not the type of perfusable vasculature. Successful constructs of perfusable vascular channels in ECM gels containing skeletal myoblasts or muscle tissues have been reported [88, 97]. However, the muscle cell density of the entire tissue is much lower than the physiological level [98] with the use of a large portion of the ECM gel. The non-functional thick ECM gel also hinders the contraction of the myotubes. Another study used the three-dimensional (3D) bioprinting technology for constructing large ehSMTs with multiple perfusable microchannels in the muscle tissues [99], but the tissues had only muscle cells and were not prevascularized. Re-

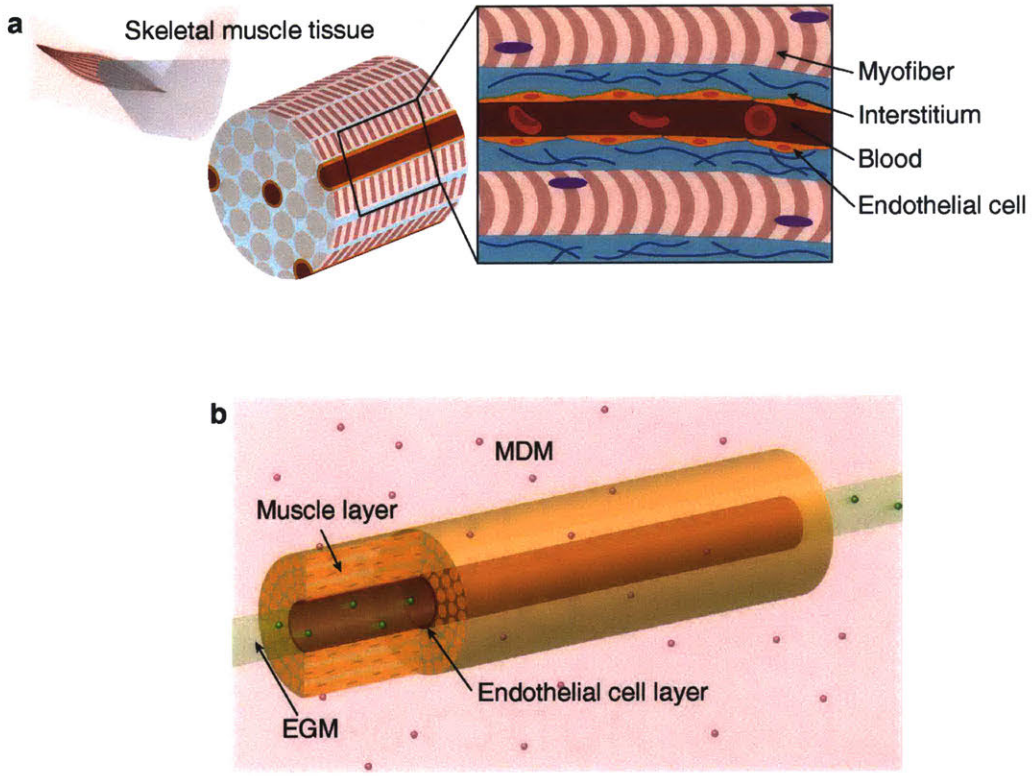

Figure 3-1: Engineered human vascularized skeletal muscle tissue with fluid compartments inspired by the *in vivo* muscle tissue structure. **a**. Extracellular fluid compartments between the blood plasma and interstitial fluid in natural skeletal muscle tissues. **b**. Design of the vascularized engineered skeletal muscle tissue to recapitulate the fluid compartments. EGM: endothelial cell growth medium, MDM: muscle differentiation medium.

cent organ-on-a-chip platforms have succeeded in modeling the fluid compartments for other organs[100, 101]. They used a synthetic membrane for separating host cells from endothelial cells, which hindered direct cell-cell interactions. In addition, using the polydimethylsiloxane (PDMS) membrane not only reduces muscle contractile performance due to an increased non-functional portion but also makes it unsuitable for implantable tissues.

To overcome the limitations of the previous works, we developed a new method for coculturing human skeletal muscle cells and endothelial cells with two separate media by creating a tubular, perfusable vasculature inside a 3D skeletal muscle tissue. Using a sacrificial molding technique, a coaxial tubular structure was constructed, in which the inner tube is covered by a confluent monolayer of endothelial cells and the outer layer consists of aligned skeletal myotubes of a physiological cell density. Endothelial cells are exposed to their matched medium EGM running through the inner tube, and the skeletal muscle cells are surrounded by differentiation medium MDM. Muscle cells and endothelial cells make contact at the tubular boundary, through which heterotypic cell-cell interactions are observed. These media separation and cell-cell interactions are achieved without using a synthetic membrane. Furthermore, skeletal muscle cells are also exposed to axial tension due to cell-mediated gel compaction, which promotes cell alignment and differentiation, while endothelial cells receive a shear force due to fluid flow through the inner tube.

By using this newly developed coculture model of vascularized ehSMTs, we investigated the integrative effects of incorporating 1) the fluid compartment for each cell type, 2) the perfusable vascular channel through the ehSMTs, and 3) the temporal coordination of coculturing timing upon the improvement of functionalities of the ehSMTs. By administrating perfusion through the compartmentalized vasculature channel, we increased the size of the ehSMTs beyond the diffusion limit. Moreover, we tested the responses of vascularized ehSMTs to myotoxic drugs. To our knowledge, this is the first work constructing multi-scaled vascularized ehSMTs under natural-like compartmentalized environments and investigating the effects of temporal and spatial environmental cues on the functionalities of vascularized ehSMTs *in vitro*.

Additionally, we increased the capillary density of the ehSMTs by promoting angiogenesis, a natural process to form new vasculatures from existing ones, to mimic the morphology and environments of capillaries in natural muscles. Capillaries are mostly aligned in the longitudinal direction of myofibers with some short interconnecting capillaries within endomysium, and their density determines the metabolic capacity by providing molecule exchange [113]. Although natural skeletal muscles have approximately six hundred capillaries per square millimeter [110], the vascularized ehSMT is designed to have a single perfusable vascular channel when it is constructed. To obtain further vascularization of the ehSMTs through angiogenesis, a pro-angiogenic factor, vascular endothelial growth factor (VEGF), is added to the perfusable vascular channel.

3.2 Materials and methods

3.2.1 Cell culture

In chapter 2, we fabricated the engineered skeletal muscle tissues composed of mouse myoblast cell line (C2C12). In this chapter, we used human primary skeletal muscle myoblasts (HSMMs) to construct ehSMTs, which can be utilized as a drug testing platform with human response and an implantable tissue. HSMMs (Lonza, Walkersville, MD) were grown in StemLife Sk medium (Lifeline Cell Technology, Oceanside, CA) supplemented with 1% (v/v) penicillin-streptomycin (PS, Sigma-Aldrich, Saint Louis, MO) and 0.2% (v/v) Normocin (InvivoGen, San Diego, CA). Human umbilical vein endothelial cells (HUVECs, Lonza, Walkersville, MD) or RFP-expressing HUVECs (RFP-HUVECs, Angio-Proteomie, Boston, MA) were cultured using endothelial cell growth media (EGM)-Plus (Lonza, Walkersville, MD) supplemented with 1% (v/v) PS and 0.2% (v/v) Normocin.

3.2.2 Fabrication of the vascularized ehSMTs

We modified a previously published protocol for constructing a solid cylindrical shape of engineered mouse skeletal muscles [27] into the fabrication of a coaxial vascularized ehSMT in a tubular shape. In short, we created a cavity by putting the 5% (w/w) gelatin (Sigma-Aldrich, Saint Louis, MO) and 10 U/mL thrombin solution (Sigma-Aldrich, Saint Louis, MO) with a stainless pin (McMaster-Carr, Robbinsville, NJ) and removing the pin when the solution is solidified. A mixture of HSMMs (15 million cells/mL) and the ECM solution, comprising 4.5 mg/mL of fibrinogen (Sigma-Aldrich, Saint Louis, MO) and 10% (v/v) growth factor-reduced Matrigel (Corning, Corning, NY), was injected into the cylindrical cavity in the gelatin sacrificial mold with insertion of a stainless pin (McMaster-Carr, Robbinsville, NJ) at the center. The diameter of this pin was smaller than the diameter of the first pin to form tubular ehSMTs. The sacrificial gelatin mold dissolved at 37°C, and released thrombin (10 U/mL, Sigma-Aldrich, Saint Louis, MO) in the gelatin solution gelated the fibrinogen in the cell mixture. The ehSMTs were incubated in growth medium composed of StemLife Sk Medium and 1 mg/mL aminocaproic acid (AA, Sigma-Aldrich, Saint Louis, MO).

Two days after ehSMT formation (Day 2), the stainless pin in the tissue was removed, which created the inner channel. Then, 4 million cells/mL of HUVECs or RFP-HUVECs were seeded into the inner channel of the tubular ehSMTs to vascularize the channel. After seeding the endothelial cells, the ehSMTs were incubated for one day with the coculture medium, comprises a half-and-half mixture of Dulbecco's Modified Eagle's medium (DMEM, 4500 mg/L glucose, Sigma-Aldrich, Saint Louis, MO) and endothelial basal medium (EBM)-Plus (Lonza, Walkersville, MD), supplemented with EGM-plus SingleQuots (Lonza, Walkersville, MD), 1% (v/v) horse serum (Sigma-Aldrich, Saint Louis, MO), 1 mg/mL AA, 1% (v/v) PS, 0.2% (v/v) Normocin, 50 ng/mL insulin-like growth factor-1 (IGF-1, Sigma-Aldrich, Saint Louis, MO), and 1x insulin-transferrin-selenium (Life Technologies Corp, Carlsbad, CA). From Day 3 to Day 8, we provided TwoM, which comprises the EGM-plus with 1%

(v/v) PS, 0.2% (v/v) Normocin, and 1 mg/mL AA in the inner channel with flow and the MDM surrounding the outer muscle layer of the ehSMTs. The MDM is composed of 2% (v/v) horse serum, 1% (v/v) PS, 0.2% (v/v) Normocin, 1 mg/mL AA, 50 ng/mL IGF-1, and 1x insulin-transferrin-selenium in DMEM. The ehSMTs of the single coculture medium condition continued to be incubated in the coculture medium until Day 8.

3.2.3 Measurement of the contractile force

We measured the contractile force of the ehSMTs using a system that was previously developed in our group [1, 27]. In brief, we stretched the cylindrical ehSMTs (2.3% strain) using the tip of the cantilever (Remington Industries, Johnsburg, IL). When the tension of the stretched ehSMTs and the elastic restoring force of the cantilever were balanced, we applied the electric field (2.5 V/mm, pulses of 1 ms each, for 3 seconds) to induce muscle contraction. The tip of the cantilever was moved to a new position of force balance by the additional contractile force during the concentric contraction. The distance between the original and new force balance positions was measured to calculate the deformation of the elastic cantilever by the contractile force. We knew the stiffness of the cantilever; thus, the deformation was calculated into the force by Hooke's law. More detailed calculations of the force are introduced in the previously published paper [1].

3.2.4 Flow in the perfusable vascular channel

Both ends of the ehSMT were anchored to a previously reported PDMS device [27] that contained the ehSMTs and reservoirs for culture medium. Through two blunt-tip needles (McMaster-Carr, Robbinsville, NJ), the inner channel of the ehSMTs in the PDMS device was connected to the microfluidic system, which consisted of a peristaltic pump (Cole-Parmer, Vernon Hills, IL) and peroxide-cured silicone tubing (Cole-Parmer, Vernon Hills, IL) containing the culture medium. Using the peristaltic pump caused a circumferential strain to the ehSMTs at 0.05 Hz by the squeezing of

the tubing that the pump created. The average circumferential strain was $\pm 2.5\%$ on Day 4 of the ehSMT formation, but because the diameter of the inner channel became smaller due to cell-mediated gel compaction, the strain was increased to $\pm 5.0\%$ on Day 8. We also calculated the shear stress applied to the endothelial cells in the inner channel by measuring the flow rate. When we assumed that the diameter of the inner channel was constant on the same day and laminar flow, the shear stress on the wall of the inner channel was 0.6 dyne/cm^2 on Day 4 and increased to 7 dyne/cm^2 on Day 8 as the flow rate remained the same and the inner channel decreased.

Fluid compartments and diffusion of the medium from the inner channel to the muscle layer of the ehSMTs were shown by flowing fluorescein isothiocyanate (FITC)-dextran solution (70 kDa, 10 μM, Sigma-Aldrich, Saint Louis, MO) in the inner channel of the vascularized skeletal muscle tissue for one hour. FITC-dextran was imaged by an Olympus IX-81 inverted fluorescence microscope (Olympus Corp., Tokyo, Japan), and the intensity was quantified by ImageJ software (NIH, Bethesda, MD). The measured intensity was normalized by the dextran intensity in the inner channel.

3.2.5 Histological analyses and immunohistochemistry

The ehSMTs were fixed with 4% paraformaldehyde (Santa Cruz Biotechnology, Dallas, TX) for 24 hours and stored in 70% ethanol. After the tissues were embedded in paraffin using standard processing techniques (Sakura VIP 5 tissue processor, Torrance, CA), they were sectioned at 4 μm and analyzed by staining techniques. Hematoxylin and eosin (H and E) staining was used to measure the fusion rate of myoblasts over time. Moreover, immunohistochemical (IHC) staining using the antibodies of laminin (Sigma-Aldrich, Saint Louis, MO) and CD31 (Abcam Inc, Cambridge, MA) allowed us to measure the myotube thickness and observe the contact between the endothelial cells and skeletal muscle cells. The slides were heat induced epitope retrieved (HIER) using citrate buffer (pH 6, Thermo Fisher TA250 PM1X, Thermo Fisher Scientific, Waltham, MA) for 20 minutes at 97°C and cooled for 20 minutes. The sections were quenched with H202 (Thermo Fisher Scientific, Waltham, MA), blocked with Rodent Block M (RBM 961 Biocare Medical, Concord, CA) for 30 minutes and in-

cubated with the primary first antibodies for 60 minutes. After being washed with Tris buffered saline and Tween (TBST, Thermo Fisher Scientific, Waltham, MA), the sections were incubated with mouse-AP/rabbit-HRP-labeled polymers for 30 minutes (Biocare Medical, Concord, CA). Labeling was achieved with 3,3'-diaminobenzidine (DAB, Fisher Scientific, Waltham, MA) or Vulcan Fast Red AP chromogen (Biocare Medical, Concord CA). The stained sections were imaged by bright field light microscopy (Aperio slide scanner, Leica, Buffalo Grove, IL).

3.2.6 Immunostaining and cell viability

The vascularized ehSMTs were fixed with 4% (w/v) paraformaldehyde (Santa Cruz Biotechnology, Dallas, TX), washed with Dulbecco's phosphate buffered saline (DPBS), and permeabilized with 0.1% Triton X-100 (Thermo Fisher Scientific, Waltham, MA). After blocking with 5% (v/v) goat serum (Sigma-Aldrich, Saint Louis, MO)/1% (w/v) bovine serum albumin (BSA, Sigma-Aldrich, Saint Louis, MO) in DPBS, the tissues were incubated with the primary antibodies of vascular endothelial (VE)-cadherin (Abcam Inc., Cambridge, MA) in 1% (w/v) BSA/DPBS, washed with DPBS, and incubated with the Alexa Fluor 568 secondary antibody (Life Technologies Corp, Carlsbad, CA) in 1% (w/v) BSA/DPBS. To stain the nuclei, Hoechst solution (Life Technologies Corp, Carlsbad, CA) was added to the tissue and washed with DPBS. Images were taken with a FluoView FV1000 series laser scanning confocal microscope (Olympus Corp., Tokyo, Japan), and the confocal z-stack images were processed using Fiji/ImageJ (NIH, Bethesda, MD).

We used a cell viability imaging kit (Blue/Green, Life Technologies Corp, Carlsbad, CA) to image the live and dead cells in the tissues, indicated in blue and green, respectively. Images were taken by using an Olympus IX-81 inverted fluorescence microscope (Olympus Corp., Tokyo, Japan), and the images were analyzed by ImageJ software (NIH, Bethesda, MD) to count the number of nuclei. Cell viability was calculated by dividing the total number of nuclei minus the number of nuclei of dead cells by the total number of nuclei. The decrease rate in the percentage of viability and contractile force in testing myotoxic drugs was calculated by dividing

the mean value of the untreated samples and the average of the samples treated with atorvastatin by the mean value of the untreated samples and then multiplying by 100. The standard error means (SEM) of this value was calculated by the following propagation of the error equation with the assumption that it is a random error:

$$\mathrm{SEM} = \mathrm{Mean} \times \sqrt{\left(\frac{\sqrt{\mathrm{SEM_{untreat}}^2+\mathrm{SEM_{treat}}^2}}{\mathrm{Mean_{untreat}}-\mathrm{Mean_{treat}}}\right)^2+\left(\frac{\mathrm{SEM_{treat}}}{\mathrm{Mean_{treat}}}\right)^2}.$$

3.2.7 PCR

PCR experiments were conducted by Dr. Tatsuya Osaki as a collaboration. To quantify muscle differentiation from the tissue, total RNA was isolated from tissues with Trizol reagent (Life Science, Waltham, MA). Reverse transcription was performed using a SuperScript VILO cDNA Synthesis Kit (Invitrogen, Waltham, MA). RT-PCR was performed with a 7900HT Fast Real-Time PCR System (Applied Biosystems, Waltham, MA) using SYBR Premix Ex Taq (Takara, Kusatsu, Japan). The primer sequences are as follows:

MyoD1-forward: 5'-CGGCCTGAGCAAAGTAAATGA-3',

MyoD1-reverse: 5'-GGCAACCGCTGGTTTGG-3',

myosin heavy chain (MHC)-forward: 5'-CCCTACAAGTGGTTGCCAGTG-3',

MHC-reverse: 5'-CTTCCCTGCGCCAGATTCTC-3',

Myogenin-forward: 5'-GTCCCAACGCAGGAGATCATT-3',

Myogenin-reverse: 5'-GCAGATTGTGGGCGTCTGTAG-3',

and CSNK2A2-forward: 5'-GAACCTTCGTGGTGGAACAAA-3',

CSNK2A2-reverse: 5'-CCTGTGCATGATTCCCTTGC-3'.

The mRNA level of CSNK2A2 as a housekeeping gene was set to 100% and used as the internal standard in all experiments. The RT-PCR experiment was repeated at least three times for cDNA prepared from at least three batches.

3.2.8 Tube formation assay

For this assay, 25 U/mL thrombin (Sigma-Aldrich, Saint Louis, MO) and 2.5 mg/mL fibrinogen (Sigma-Aldrich, Saint Louis, MO) dissolved in DMEM (Sigma-Aldrich,

Saint Louis, MO) was placed in a 24-well plate (VWR Scientific, Pittsburgh, PA) with 300 μL/well and incubated for an hour. Then, RFP-HUVECs (Angio-Proteomie, Boston, MA) were mixed with the conditioned medium and seeded onto the gelated fibrin in the plate. The conditioned medium was the coculture medium incubated for two days with the vascularized ehSMTs from Day 2 and Day 5 of the ehSMT formation. The HUVECs were incubated again for 36 hours and imaged by the Olympus IX-81 inverted fluorescence microscope (Olympus Corp., Tokyo, Japan). The images were analyzed with WimTube online software (Onimagin Technologies SCA, CÃşrdoba, Spain).

3.2.9 Measurement of permeability

We measured the permeability of the perfusable vascular channel as described previously [97]. In short, we put the FITC-dextran solution (70 kDa, 25 μM, Sigma-Aldrich, St. Louis, MO) into the inner channel and measured the diameter of the inner channel and the average intensities of the tissues at the initial and final time points using ImageJ software (NIH, Bethesda, MD). To calculate the permeability, we assumed that the cross-section of the vascular channel was a circle, and the detailed equation can be obtained from the reference [97].

3.2.10 Statistical analyses

Statistical analyses were conducted using Student's t-test, ANOVA with Tukey's post-test and ANOVA with Bonferroni's post-test. Data were considered statistically significant if the P-value was 0.05 (*), 0.01 (**), or 0.001 (***).

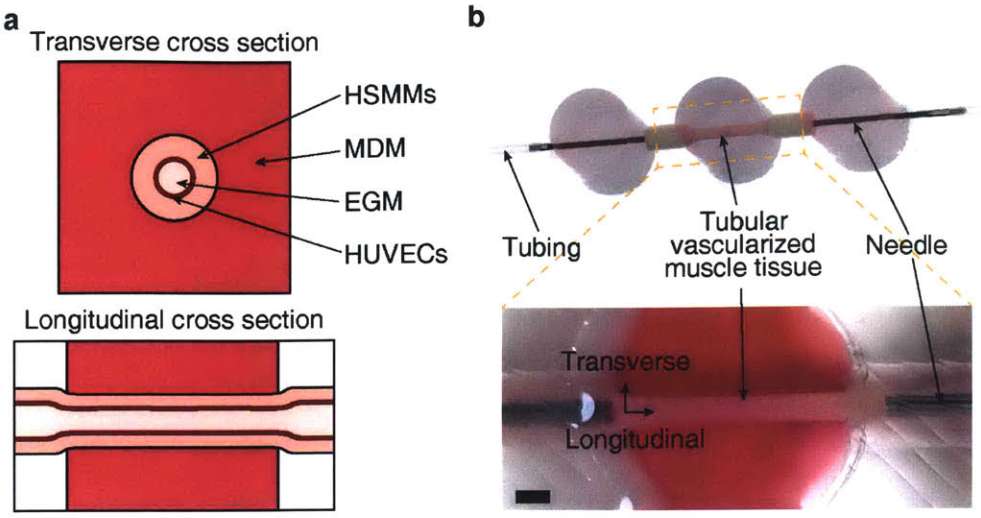

Figure 3-2: **a.** Schematics of transverse and longitudinal cross-sections of the engineered tissue. HSMMs: human skeletal muscle myoblasts, HUVECs: human umbilical vein endothelial cells. **b.** Image of the engineered vascularized skeletal muscle tissue. The inner vascular channel is connected to a microfluidic system through needles to produce fluid flow. The scale bar represents 1 mm.

3.3 Results

3.3.1 Two culture media are compartmentalized with a coaxial tubular tissue construct

To meet the three functional requirements for coculturing (separation of two media; lumping of the same type of cells; and placing the two cell types within the reach of heterotypic cell-cell interactions), we designed a coaxial vascularized ehSMT in a tubular structure (Fig. 3-1**b**). The outer layer consists of human skeletal muscle tissue, and the inner layer is a perfusable vascular channel comprising a monolayer of endothelial cells. The muscle cells and endothelial cells contact at the boundary of the inner and outer layers. This design allowed us to administer the two separate culture media: EGM to endothelial cells through the perfusable vascular channel and MDM to muscle cells in the medium space surrounding the outer muscle layer (Fig. 3-2**a**). The inner channel of the coaxial construct was connected to needles at both ends, which were further connected to tubing and a microfluidic pump that circulated

EGM through the inner channel and provided the endothelial cells with a shear stress (Fig. 3-2**b**). Both EGM and MDM were replaced by fresh media every day. The outer muscle layer comprised HSMMs and ECM with 4.5 mg/mL fibrinogen and 10% (v/v) Matrigel when the cells were seeded. The inner vascular channel comprises HUVECs seeded into the inner channel by suspending them in EGM without adding ECM.

The longitudinal cross-sections of the vascularized ehSMT showed that the inner channel was well covered with a monolayer of HUVECs (Fig. 3-3**a**). The HUVECs covering the inner channel were aligned in the longitudinal direction of the tissue (Fig. 3-3**b**). Furthermore, those HUVECs directly contacted the skeletal myotubes or adhered to the inner wall of the muscle tissue. Unlike the prior works using permeable synthetic membranes [100, 101] for separating them, this method allows the muscle cells and endothelial cells to be placed closely together, so that the two sides can directly interact. When we seeded the endothelial cells into the inner channel of the ehSMT, the contractile force was much higher than when seeding them at the reservoir bottom approximately 3 mm away from the ehSMT (Fig. B-2).

Two cell culture media for each cell type were compartmentalized by the tubular tissue and replaced with fresh EGM and MDM every day. The MDM and EGM in this study had different colors, generally due to differences in the concentrations of phenol red (MW: 354 Da), 16 mg/L and 1.17 mg/L, respectively. We confirmed that they maintained their colors after one day (Fig. B-3**a**-**d**). Despite the fact that the two media maintained their colors, the diffusion experiment using the fluorescein isothiocyanate (FITC)-dextran (70 kDa, 10 μM) with EGM in the inner channel (Fig. 3-4) showed that some soluble factors were still able to diffuse through the vasculature and the outer muscle layer. However, the intensity of the FITC-dextran was still almost zero in the outer medium space. This reconfirmed that the two media remained different, which was achieved by the high cell density of ehSMTs, flow in the inner channel, a large volume of outer medium space, and daily media replacement to keep the two media from mixing.

This coaxial, double layer construct was made by using a sacrificial molding technique [27]. The existing method for forming a fascicle-like 3D skeletal muscle tissue

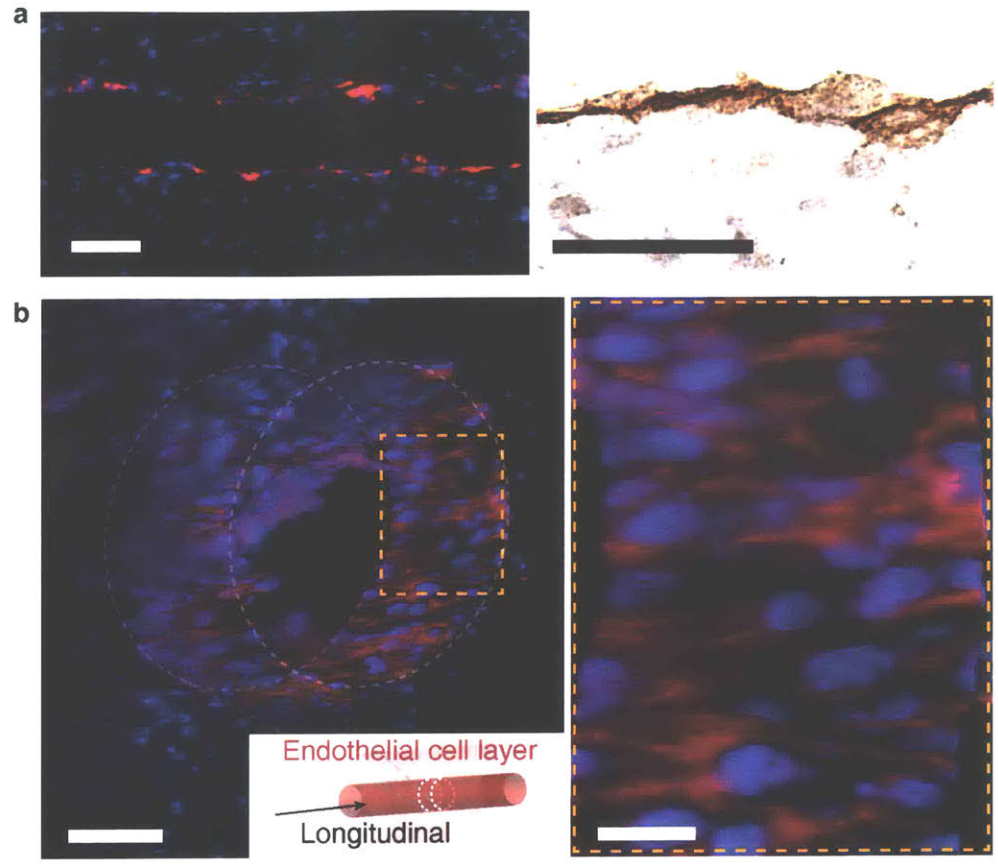

Figure 3-3: **a**. Sectioned slides in the longitudinal direction to show that endothelial cells cover the inner channel and are very close to muscle cells. In the right image, blue and red indicate the nucleus and RFP-expressing HUVECs, respectively. The scale bar represents 100 μm. In the left image, dark brown and light purple indicate endothelial cells and the nucleus, respectively. The scale bar represents 20 μm. **b**. Confocal image of VE-cadherin (red) of the endothelial cells in the perfusable vascular channel and nucleus (blue). Scale bars represent 100 and 10 μm.

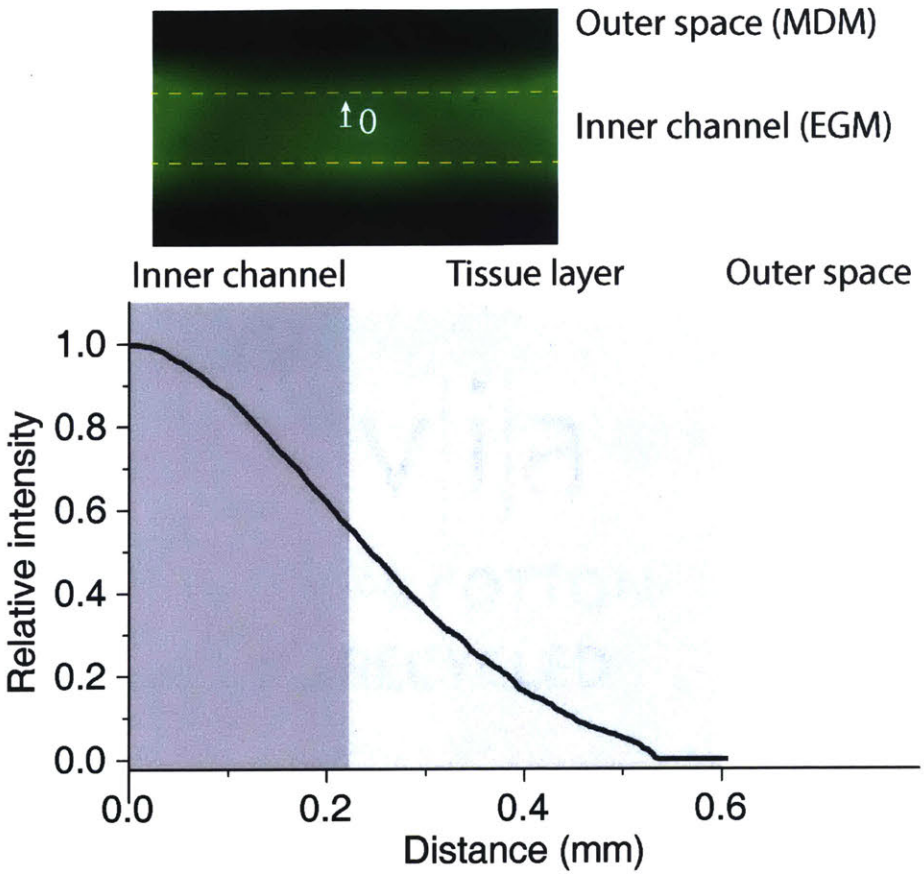

Figure 3-4: Fluids compartments are shown by flowing FITC-dextran solution (70 kDa, 10 μM) in the inner channel of the vascularized muscle tissue for one hour. The boundary of the inner channel is indicated by dashed lines.

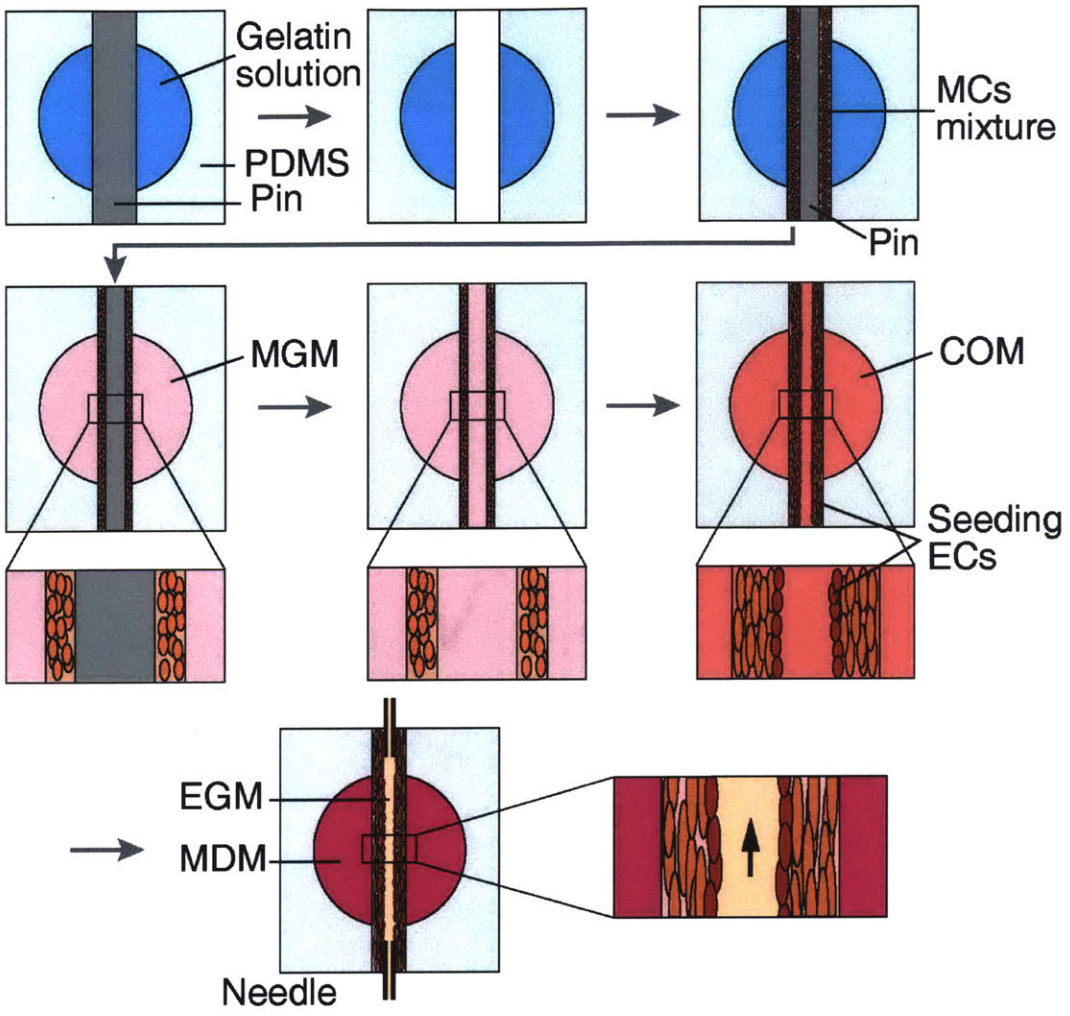

Figure 3-5: Fabrication of an engineered human vascularized skeletal muscle tissue. Skeletal muscle cells (MCs) mixed with the extracellular matrix are injected into a cavity in a gelatin sacrificial mold with a pin to construct 3D tubular engineered muscle tissues. The gelatin is melted in the incubator and removed by a medium change. When the MCs form a solid tissue in the muscle cell growth medium (MGM), the pin in the tissue is removed, and endothelial cells (ECs) are seeded into the inner channel. One day after seeding endothelial cells, needles are connected to a microfluidic system to supply the two separate media with flow. Endothelial growth medium (EGM) for ECs and muscle differentiation medium (MDM) for MCs can be compartmentalized by tubular tissue.

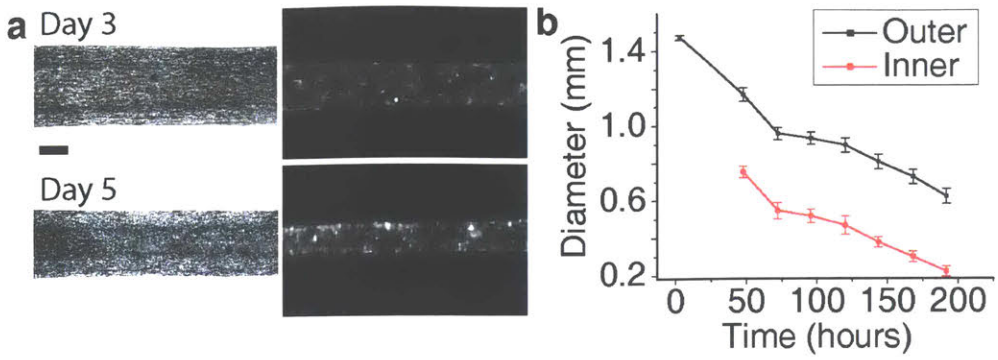

Figure 3-6: **a**. Phase-contrast microscopic images of the muscle tissue in a tubular shape (left) and RFP-expressing HUVECs in the inner channel of the muscle tissue (right) at three days (Day 3) and five days (Day 5) from the muscle tissue formation. The scale bar represents 300 μm. **b**. Outer and inner diameters of the vascularized tissue are decreased over time by cell-mediated compaction and degradation of the extracellular matrix. SEM. n = all 13.

[27] was extended to create a coaxial structure using two stainless pins with different diameters (Fig. 3-5). We embedded the thicker stainless pin, with a diameter of the desired tissue size, in a solution of 5% gelatin and 10 U/mL thrombin in muscle growth medium (MGM). When the gelatin solution was solidified in 4°C, the pin was removed to make a cylindrical cavity in the solid gel. Then, this cylindrical cavity was filled with HSMMs with 4.5 mg/mL fibrinogen in MGM and 10% (v/v) of growth factor-reduced Matrigel. With this cell solution, a thinner pin was placed at the center to create an inner channel in the muscle tissue. When the cell solution was fully solidified to form the muscle tissue in an incubator, the thinner pin was extracted linearly, and HUVECs suspended in the EGM were seeded into the inner channel of the tubular ehSMTs. The seeding cell density of the muscle layer was 15 million cells/mL, which is in the physiological range (10-500 million cells/mL), and the ratio of seeded HSMMs to HUVECs was 5 to 1. After the seeded HUVECs were incubated for one day for attachment to the surface of the inner channel, the channel was connected to the microfluidic system to provide the EGM with flow, and the MDM was used to fill the reservoir outside the tissue.

The constructed vascularized ehSMTs became thinner over time because of the cell-mediated gel compaction [27] (Fig. 3-6**a**). The changes in the inner and outer

diameters of the tubular tissue were characterized for 8 days (Fig. 3-6**b**). The ehSMT shown is a smaller-scale model, which measured approximately 1.5 mm in outer diameter and 8 mm in length in the beginning. Due to cell-mediated gel contraction, the diameter was reduced to approximately 600 μm on Day 8 (Fig. 3-6**b**). However, since muscle cells at both ends of the tissue adhered to the PDMS reservoir, the length was not reduced but tension was generated in the longitudinal direction. This mechanical tension aligns myoblasts and promotes muscle differentiation [94, 102].

3.3.2 Use of two compartmentalized media with perfusable vasculature improves muscle functionalities and scales up the ehSMTs

To quantify the effects of the use of two separate media (TwoM), we measured contractile force and evaluated myotube morphology and muscle differentiation. Comparisons were made between single coculture media (COM) and TwoM under the same flow conditions (Fig. 3-7**a**). The difference is that EGM and MDM were supplied for endothelial cells and skeletal muscle cells, respectively, in TwoM, while the same coculture media was provided to both in single COM. We seeded endothelial cells on Day 2 of the ehSMT formation and provided TwoM and single COM with inner channel flow from Day 3 through Day 8. The wall shear stress was estimated based on the flow rate and the inner channel diameter. The shear stress was 0.6 dyne/cm^2 on Day 4 and increased to 7 dyne/cm^2 on the last day because the tissue became narrower during the incubation (Fig. 3-6**b**).

As shown in Fig. 3-7**b**, the contractile force of TwoM was approximately 76% higher than that of single COM. The morphological evaluation revealed that the fused myotubes in the ehSMTs were well aligned in the longitudinal direction of the tissues with high volumetric cell density in both single COM and TwoM cases (Fig. 3-7**c**), but TwoM produced thicker myotubes on average than single COM (Fig. 3-7**c**, **d**). Furthermore, the evaluation of differentiation using PCR indicated that the expression of MyoD and MHC, which are muscle differentiation-related genes, increased when

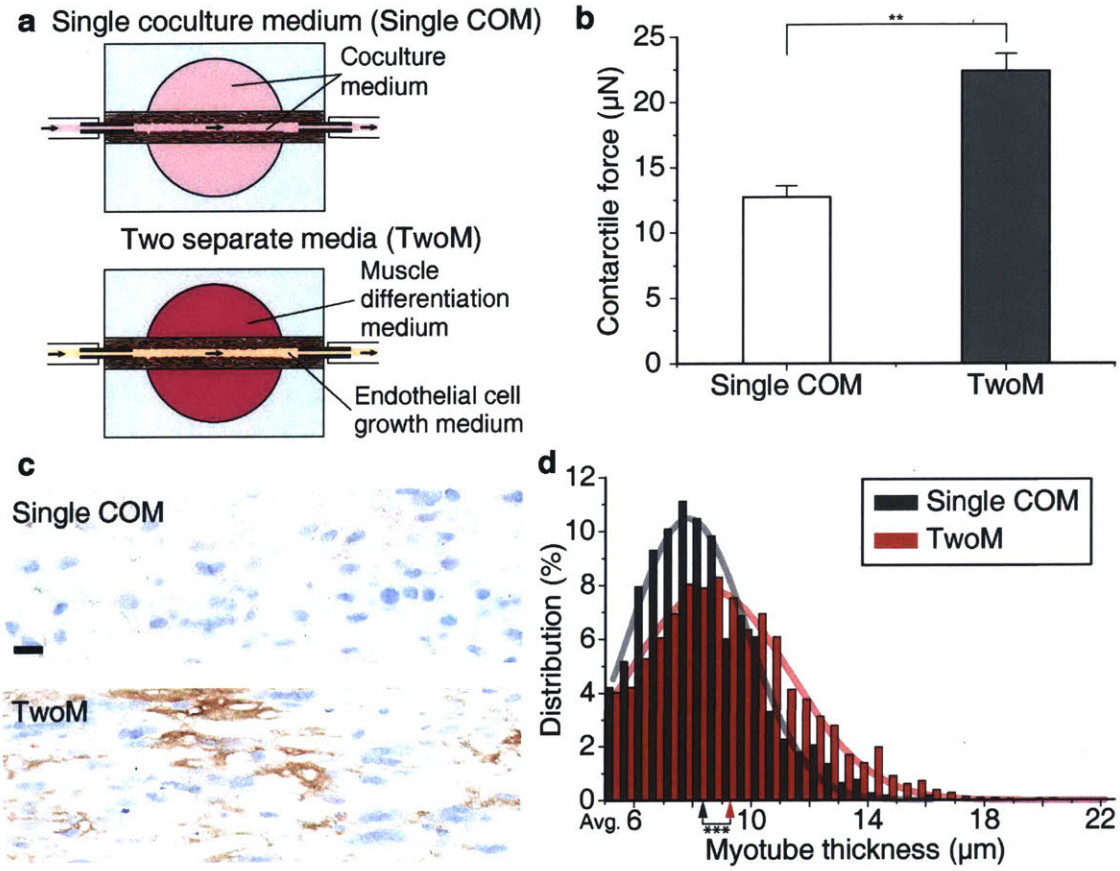

Figure 3-7: Fluid compartments for using the two different culture media for each cell type enhance the functionalities of the vascularized skeletal muscle tissues. **a**. Tested conditions using the coculture medium (COM) both inside and outside of the tissue (Single COM) or using the two separate media (TwoM) with the muscle differentiation medium surrounding the outer skeletal muscle layer and the endothelial cell growth medium in the inner vascular channel. Both conditions provide fluid flow in the inner channel. **b**. Using TwoM increased the contractile force compared to that using a single COM on Day 8. SEM. n = 3 and 10. Student's t-test. **c**. Histological sectioned images of the muscle tissues in the culture conditions of single COM (top) or TwoM (bottom). Laminin and nuclei were stained in brown and blue, respectively. The scale bar represents 10 μm. **d**. The thickness of myotubes, n = 1548 and 3585. Student's t-test. $^{**}P < 0.01$ and $^{***}P < 0.001$.

TwoM was used (statistically not significant, Fig. B-4). These results showed that the contractile performance and differentiation of the skeletal muscle cells were more improved by using TwoM than by using single COM.

Instead of simply adding endothelial cells to the ehSMT by mixing, we formed a perfusable vascular channel. This provided a more optimized medium with flow to the endothelial cells and delivered a fresh medium into the muscle tissue, similarly to the blood vessels of the body. This perfusable vasculature and flow in the channel allowed us to build a subcentimeter-sized large ehSMT (Fig. 3-8**a**), which had an average outer diameter of 2.2 ± 0.038 mm (SEM, n = 2) on Day 8. The viability of cells in the large-scale vascularized ehSMTs was higher than 80% at both the edge and center parts of the tissues (Fig. 3-8**b**, **c**). The viability of the small-scale ehSMT with an average outer diameter of 600 μm had almost the same viability as the large one. However, the viability of the large-scale tissues was significantly lower at the center if the vasculature and medium flow were not created (Fig. B-5). This result shows that the constructed ehSMTs with TwoM can be scalable, ranging from micrometer to subcentimeter scales, through the perfusable vascular channel and flow through it.

3.3.3 Timing of the vascularization influences the functionalities of the muscle tissues and endothelial cells

Each stage of muscle differentiation is governed by different signaling pathways [103], thus, the results of the coculture could be affected by the timing of seeding endothelial cells relative to the muscle differentiation stage. Since the newly developed technique enables seeding the two cell types not only spatially (B-2) but also temporally separated, we investigated the appropriate timing to initiate the coculture to create high-performance ehSMTs. Between Day 2, the day of producing the inner channel in the ehSMTs, and Day 8, the last incubation day, we chose Day 2 and Day 5 as testing time points. These time points had a sufficient time interval to show a significant difference in fusion rate (Fig. 3-9 and B-6, [90]) and an adequate interaction time between muscle and endothelial cells. To examine the effects of the coculture

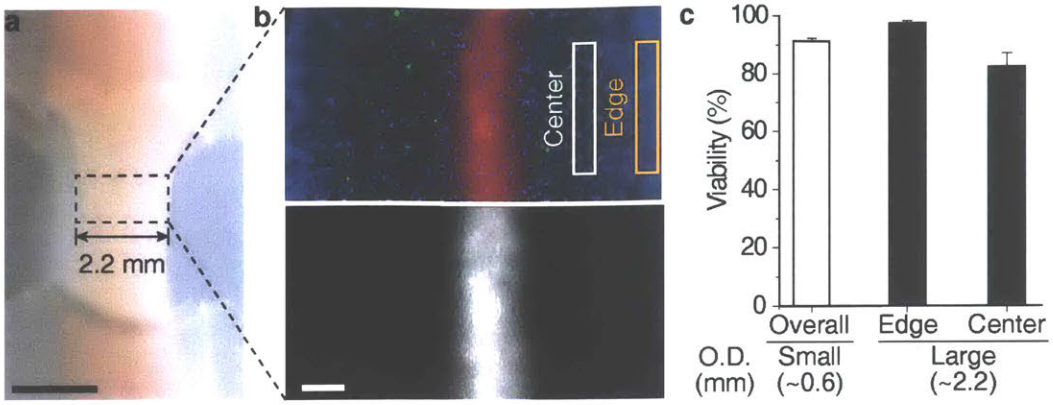

Figure 3-8: **a**. Image of the large-size vascularized ehSMT with TwoM. The scale bar represents 3 mm. **b**. Fluorescent images of the vascularization of the large-size ehSMTs. Red, green, and blue in the combined fluorescent image (top) indicate RFP-expressing HUVECs, dead cells, and nuclei, respectively. The black and white image (bottom) shows RFP-expressing HUVECs in the tissue. The scale bar represents 250 μm. **c**. Viability of the large-size vascularized ehSMTs with an outer diameter (O.D.) of approximately 2.2 mm and the small-size one with the O.D. of approximately 0.6 mm were both greater than 80% when the vascularized ehSMTs were under TwoM with flow. SEM. n = 2, 4, 3.

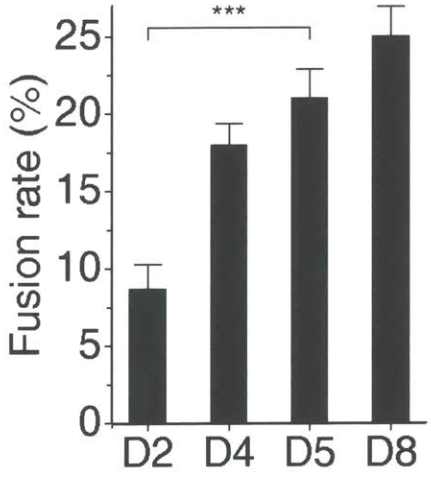

Figure 3-9: Fusion rate of myoblasts over time in the engineered skeletal muscle tissues, SEM. n = all 9. ANOVA with the Bonferroni post-test. $^{***}P < 0.001$.

timings on the functionalities of the ehSMTs, we seeded endothelial cells into the inner channel at Day 2 (CO2) and Day 5 (CO5) of the ehSMT formation. Additionally, the ehSMTs with only muscle cells (MC) were compared to determine the effect of the coculture. Because the endothelial cell layer could influence diffusion from the inner channel to the muscle tissue, the use of TwoM with different vascularization timings inevitably provided different chemical environments to the cells. Therefore, we used COM in both fluid compartments for all the conditions (MC, CO2, and CO5 conditions) in Fig. 3-10 and 3-11 to investigate the effects of the coculture starting time under the same chemical conditions. As a result, the coculture from the earlier stage of muscle differentiation (CO2) induced higher contractile force and thicker myotubes than did the CO5 and MC conditions (Fig. 3-10**a**, **b**, and B-7). In the PCR results, the expression of the muscle differentiation markers (MyoD, MHC, and Myogenin) was higher in the CO2 condition than in the MC condition (Fig. B-8**a**). However, unlike the previous results for the contractile force and myotube thickness, the mRNA expression of the differentiation markers was higher in the CO5 condition than in the CO2 condition, although this difference was not statistically significant (Fig. B-8**b**).

We also investigated the effect of coculture initiation timing on endothelial cells. In both CO2 and CO5 conditions, we could not observe sprouting of endothelial cells into muscle cells, and we found no significant difference in endothelial cells in the inner channel between the two conditions (Fig. B-9**a**, **b**). To further examine the effect of the coculture timing on the reorganization stage of angiogenesis, we performed a tube formation assay of endothelial cells using the conditioned media (Fig. 3-11). We seeded endothelial cells onto the fibrin gel and cultured them for 36 hours in the conditioned medium (CM) that was incubated with the vascularized ehSMTs for two days from Day 2 (CO2 CM) and Day 5 (CO5 CM), respectively. The results showed that the CO2 CM promoted more vascular network formation than the CO5 CM in terms of the coverage area, total tube length, and number of loops. Therefore, we could examine how the timing of starting the coculture with respect to the muscle differentiation stage influences the functionalities of muscle cells and endothelial cells.

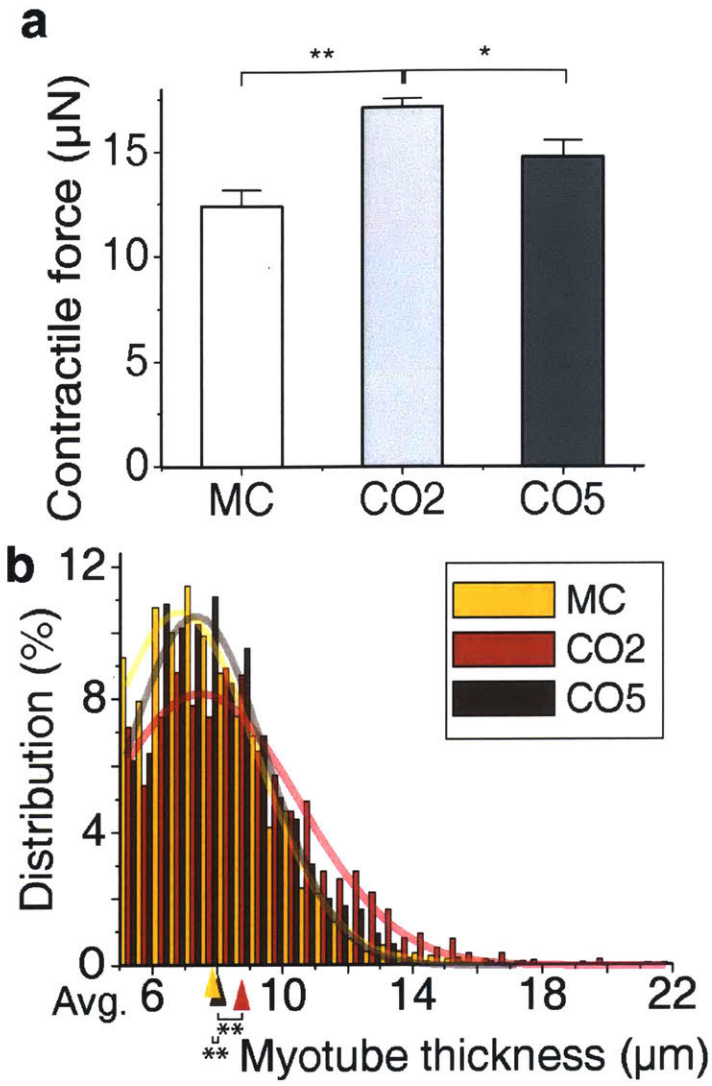

Figure 3-10: Effects of the timing of vascularization with respect to muscle differentiation. **a**. The contractile force of the engineered tissues made of only muscle cells (MC) or muscle cells with endothelial cells from Day 2 (CO2) or Day 5 (CO5) of the muscle tissue formation. SEM. n = 4, 9, and 3. **b**. Distributions of the myotube thickness in the engineered tissue sections in MC, CO2, and CO5 conditions. Triangles at the bottom indicate averages of the thickness for each condition. n = 2556, 2331, and 956. ANOVA with the Tukey post-test (**a**, **b**). $^{*}P < 0.05$, $^{**}P < 0.01$.

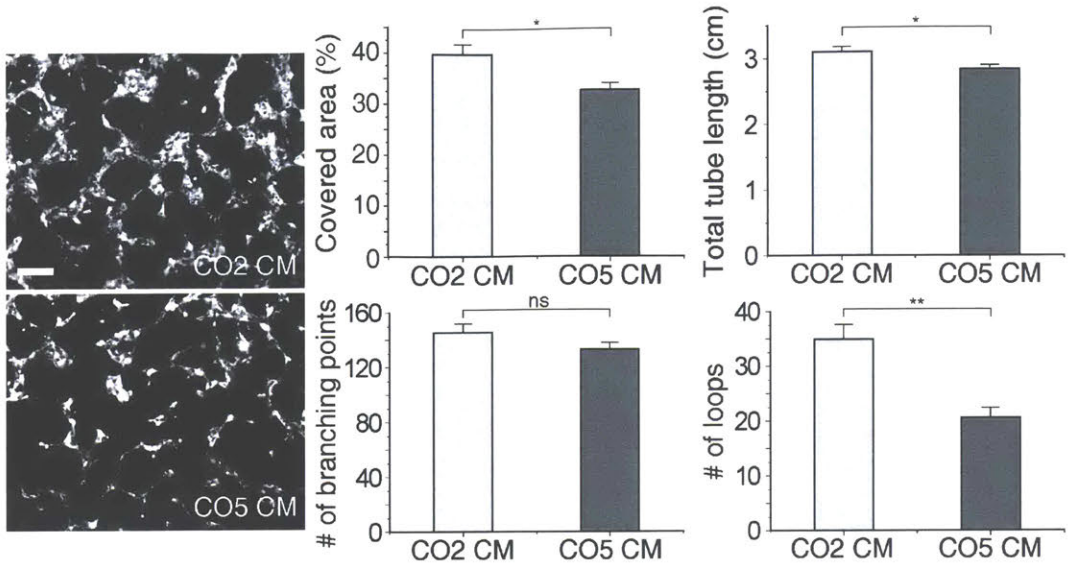

Figure 3-11: Results of the tube formation assay of endothelial cells on fibrin gel in the conditioned medium (CM). Fluorescent images of RFP-expressing HUVECs in the conditioned coculture medium (left) were analyzed (right). The coculture medium was incubated with the muscle tissues for two days from Day 2 (CO2 CM) and Day 5 (CO5 CM). The scale bar represents 250 μm. SEM. n = 49 and 21. Student's t-test. $^{*}P < 0.05$, $^{**}P < 0.01$ and ns, not significant.

Although the PCR results showed oppositely, we found that starting the coculture before HSMMs were fused at the early differentiation stage was more favorable for muscle contractile force, myotube thickness, and vascular network formation. For these reasons, we performed the previous experiments (Fig. 3-7) under the condition of seeding endothelial cells on Day 2 of ehSMTs.

3.3.4 The engineered human skeletal muscles are applicable in the drug testing

By using the vascularized ehSMTs, we examined the effect of a myotoxic drug on viability and the contractile force of vascularized ehSMTs by adding atorvastatin. Although the mechanism underlying statin-induced muscle damage remains unclear, the results of many clinical trials [104, 105] and *in vitro* experiments [26, 106] show solid evidence that statins cause myotoxicity in a dose-dependent manner, especially

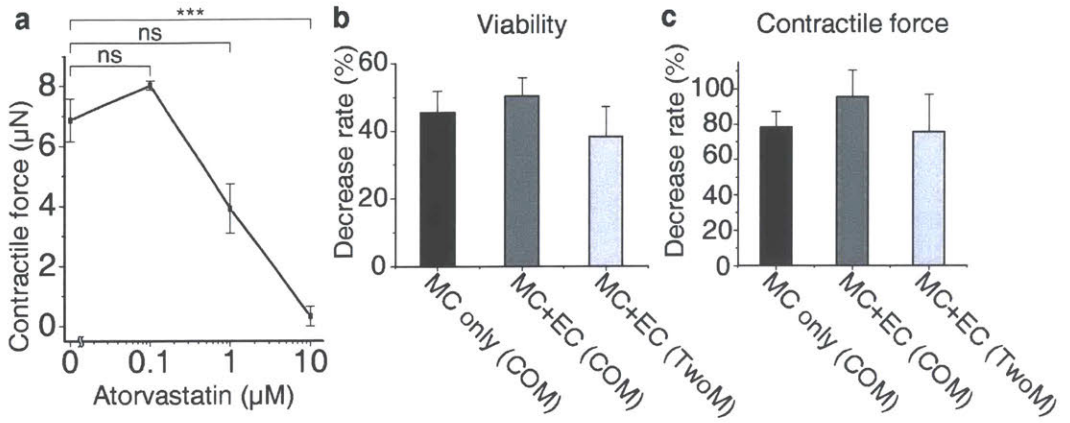

Figure 3-12: Using vascularized ehSMTs as a drug testing platform. **a**. The contractile force of the vascularized muscle tissues cultured in the coculture medium (COM) with 0 to 10 μM atorvastatin for three days from Day 3 of the tissue fabrication. SEM. n = 7, 2, 3, and 3. ANOVA with the Bonferroni post-test. **b, c**. Decrease rate in cell viability (b) and the contractile force (c) of the ehSMTs, comprising muscle cells only (MC only) or muscle cells with endothelial cells (MC+EC) in the coculture medium (COM) or the two separate media (TwoM), by culturing with 10 μM atorvastatin for three days. SEM. n = 3, 3, and 2 (**b**, untreated). n = 4, 5, and 4 (**a**, atorvastatin-treated). n = 2, 7, and 2 (**b**, untreated). n = 4, 3, and 4 (**b**, atorvastatin-treated). $^{***}P < 0.001$, and ns, not significant.

when the concentration is higher than 0.1 μM. This drug is also known to be critically toxic to endothelial cells when it is higher than 10 μM [107, 108].

To utilize the vascularized ehSMTs for testing this toxicity, we treated them with atorvastatin from Day 3 to Day 6 of the ehSMT formation and showed that the contractile force of the vascularized skeletal muscle tissues in the coculture medium was significantly decreased at the high concentration (10 μM) (Fig. 3-12**a**). As high-dose atorvastatin is known to be toxic to both cell types, 10 μM of this drug was more toxic to both viability and contractile force when the ehSMTs were vascularized (Fig. 3-12**b**, **c**, statistically not significant). We also showed that the cell culture condition influences susceptibility to drug toxicity (Fig. 3-12**b**, **c**, statistically not significant), as it is known to be more critical when the cells are cultured under less optimized culture conditions [109]. By testing the myotoxic drug with our vascularized ehSMTs, the high-dose toxicity of atorvastatin was successfully reproduced in various conditions by quantifying their viability and contractile performance.

3.3.5 Further vascularization of engineered skeletal muscle tissues is achieved by inducing angiogenesis

Although we successfully achieved de novo formation of a perfusable blood vessel, defined as vasculogenesis, in the ehSMTs (Fig. 3-3), the capillary density of the ehSMTs was still insufficient compared to natural skeletal muscles (approximately 600 capillaries per square millimeter [110]), and more investigation was still needed for the efficient formation of capillaries in engineered tissues [111]. As *in vivo* adult muscles increase their capillary density mostly through angiogenesis [112], we added 50 ng/mL of VEGF to promote angiogenesis from the main vascular channel into the muscle tissue layer. VEGF is known as the most commonly used pro-angiogenic factor to stimulate the angiogenic sprouting of endothelial cells [113, 114]; thus, it was supplemented with EGM of TwoM in the vascular channel for three days from Day 3. As a result, sprouting of endothelial cells from the inner vascular channel into the muscle tissue layer was well induced (Fig. 3-13**a**). Notably, similar to capillaries in natural skeletal muscles, the sprouted endothelial cells in the muscle layer (Fig. 3-13**b**) were mostly aligned in the longitudinal direction of both myotubes (Fig. 3-7**c**) and eSMT (Fig. 3-2**b**) with some short vertical branches (indicated by orange arrows in Fig. 3-12**b**). At the same time, we also observed many angiogenic sproutings near the perfusable vascular channel, which were still short and mostly grew vertically from the monolayer (Fig. 3-12**c**). Moreover, lumen formation of sprouted endothelial cells was seen in the muscle layer (Fig. 3-12**d**). These results demonstrated that this further vascularized ehSMT has morphologically similar vascular networks with natural skeletal muscles on top of the perfusable vascular channel and allows access to the two main processes of blood vessel formation, namely, vasculogenesis and angiogenesis, in *in vitro* skeletal muscles. To the best of our knowledge, this study is the first to reproduce both vasculogenesis and angiogenesis *in vitro* directly in contractile ehSMTs with a physiological level of muscle cell density.

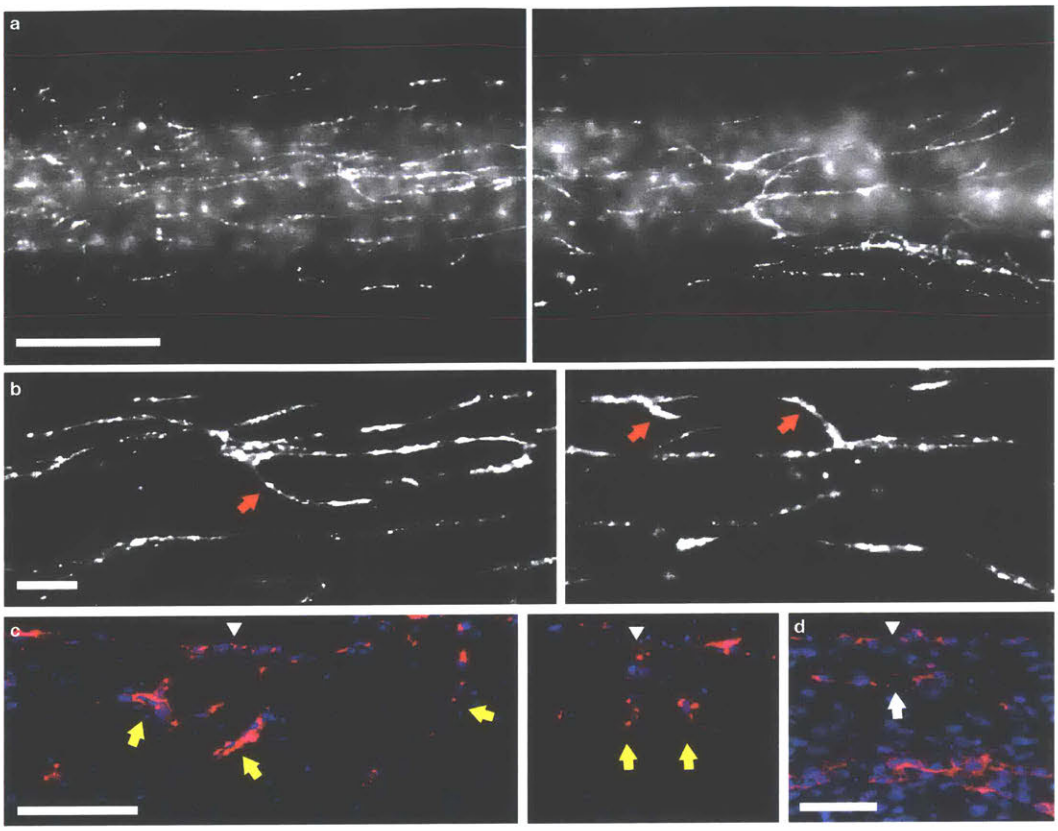

Figure 3-13: Further vascularization of the ehSMTs. **a**. Induction of angiogenic sprouting of RFP-expressing HUVECs by adding the 50 ng/mL of vascular endothelial growth factor to the inner channel is shown in the top view images of the 3D vascularized ehSMTs cultured in TwoM. Red lines indicate the outer boundary of the muscle tissue layer. The scale bar represents 500 μm. **b**. Branches of sprouted RFP-expressing HUVECs in the muscle tissue layer were mostly aligned in the longitudinal direction of the ehSMTs (horizontal direction of the images) with some short vertical branches (yellow arrows). The scale bar represents 100 μm. **c**, **d**. Angiogenic sprouting (yellow arrows in **c**) from the endothelial monolayer in the inner channel (top side, white triangles) into the muscle tissue layer and lumen formation (white arrow in **d**) were shown in the sectioned slides of the vascularized ehSMTs. Blue and red indicate the nuclei and RFP-expressing HUVECs, respectively. Scale bars represent 100 μm (**c**) and 50 μm (**d**).

3.4 Discussions and future directions

3.4.1 Main contributions

This thesis reports the development of novel vascularized ehSMTs incorporating two separate media to recapitulate the extracellular fluid compartments in the body and solve the incompatible media problem for coculturing muscle cells and endothelial cells. Although using MDM alone induced apoptotic behavior in endothelial cells (Fig. B-1**a**), using TwoM allowed us to create a perfusable channel covered with a monolayer of endothelial cells (Fig. 3-3**a**, **b**). At the same time, the use of TwoM was able to improve the contractile performance of the ehSMTs by 76% compared to using single COM (Fig. 3-7**b**). Not only the chemical cues but also the appropriate mechanical cues for each cell type were successfully delivered to improve their functions by administering an alignment of myotubes in the longitudinal direction (Fig. 3-7**c**) and shear stress by flow for endothelial cells. Moreover, the newly developed ehSMTs allow spatial (Fig. B-2) and temporal (Fig. 3-10) control of the interactions between skeletal muscle cells and endothelial cells. In particular, the effects of vascularization timing relative to muscle differentiation were addressed in this investigation for the first time. Furthermore, we showed that this platform can be scaled up for constructing the ehSMTs of subcentimeter size (Fig. 3-8).

Notably, this study enhanced the potential of two important applications of ehSMTs, namely, large-size implantable tissues and small-size drug-testing platforms, by using the single scalable vascularization platform. To create a successful and well-functioning implantable skeletal muscle tissue, ehSMTs need 1) prevascularization with a perfusable vasculature for prompt blood perfusion after implantation [115], 2) a high muscle cell density so as not to hinder muscle contraction by the non-contractile stiff gel [33], 3) natural ECM or synthetic biodegradable polymers as a scaffold [116] but no synthetic membrane between the two cell types, and 4) a natural-like microstructure, such as alignment of skeletal muscles [117]. Although previously, prevascularized ehSMTs have been implanted into mice[22, 118, 119] and have revealed that endothelial cells in the ehSMTs promotes blood perfusion and contractile

performance *in vivo*, the construction of a perfusable vasculature in the contractile ehSMT with a high muscle cell density has not yet been achieved. To the best of our knowledge, the vascularized ehSMT in this study is the first that meets all four requirements to be utilized in implantation. In addition, the ehSMTs were even able to be further vascularized by the addition of VEGF (Fig. 3-13), which could make them more advantageous due to a high capillary density after the implantation. However, more studies of the actual implantation of ehSMTs and constructing much larger ehSMTs with multichannels for VML patients are required to practically use them in the future.

3.4.2 Discussions for results

We obtained improvements in muscle contractile force and differentiation by providing TwoM (Fig. 3-7), and this result may have occurred through favorable cell culture conditions for muscle differentiation by the incorporation of MDM, which is one of the TwoM. Consequently, the contractile force of the vascularized tissues in TwoM was more similar to that of the muscle-only tissues grown in MDM (30.5 ± 2.37 μN, n = 5, SEM) than in single COM. However, using TwoM induced a slightly lower contractile force than using MDM because EGM from the inner channel (Fig. 3-4) may interfere with muscle differentiation (Fig. B-1b). The improved functionalities are also due to interactions between skeletal muscle cells and endothelial cells. A previous study has shown that endothelial cells improve muscle differentiation through Angiopoietin-1/Neuregulin-1/ErbB2 signaling [88]. In addition to paracrine signaling between endothelial cells and skeletal muscle cells, our results (Fig. B-2) demonstrate that close contact and interaction might play an important role in improving the contractile force. Thus, further investigation of mechanical and biochemical interactions between skeletal muscle cells and endothelial cells will also help to answer biological questions in the human developmental process and to elucidate regeneration.

We also compared the amount of diffused FITC-dextran (70 kDa) from the inner channel to the muscle tissue layer that passed through the endothelial cell layer. The results showed that the dextran was less diffused into the muscle tissue layer when

TwoM was provided compared to when the COM without flow was used (Fig. B-10). This is probably due to the influence of the application of a shear stress by flow, which is known to have a critical role in decreasing the permeability of vasculature [122]. However, the permeability that we obtained with flow (Fig. B-10) was higher than the values of the *in vitro* vasculature from other studies in acellular collagen gels [97, 122]. This may be because muscle cells made the vasculature more leaky, as it was shown that the permeability was increased approximately eight times when the vasculature was constructed in the C2C12-containing collagen gel [97], and we even tested it with much a higher muscle cell density. Previously, the effects of the muscle cells on the function of endothelial cells have shown in detail that C2C12 induces more angiogenesis through Angiopoietin-1 via Angiopoietin-1-Tie2 signaling [88]. Nonetheless, the exact mechanism of the increased permeability of the vasculature through paracrine signaling with muscle cells needs to be elucidated through more future studies.

Although we significantly improved the function and architecture of the ehSMT, these features may still not be sufficient to fully mimic the complex environment of natural muscles. For example, the current ehSMTs do not include immune cells, fibroblasts, motor neurons, and other stromal cells. In particular, constructing more natural-like ECM in vascularized ehSMTs, such as the basement membrane and the endomysium between myofibers and capillaries, will enhance the separation of the two media to further improve the functionalities of the two cell types by reducing the diffusion of the media through the tissues. Additionally, the EGM and MDM that we used to mimic the extracellular fluid compartments in the body are different from real body fluids. In future studies, ehSMTs will become more similar to natural muscles if these other types of cells are incorporated into the platform and make the culture media more similar to the real ones.

3.4.3 Future applications

This newly developed platform for vascularized ehSMTs can be utilized as *in vitro* skeletal muscle models or drug testing platforms, which can closely mimic the architectures and heterotypic cell-cell interactions of natural muscles by incorporating a

perfusable vasculature, fluid compartments, and appropriate mechanical cues. Additionally, the platform enables us to test key functions of the vascularized ehSMTs, including the contractile force, myotube fusion rate, myotube thickness, and permeability of the vasculature. These features will contribute to testing the toxicity and effectiveness of drugs, particularly affecting those functions and both cell types. Additionally, drugs are commonly delivered by oral, subcutaneous, intravenous, or intramuscular administration, but only the intramuscular injection has been simulated with the ehSMTs [120]. Because our ehSMTs contain an *in vitro* perfusable vasculature with the fluid compartments, they could be used as a novel drug testing device to study intravenous and oral drug delivery.

The most representative alternative to creating a similar structure to our tubular 3D tissues is the 3D bio-printing. Unlike our platform, which can make only a straight channel by using a stainless pin, 3D bio-printing can construct the channel in the tissues, with more complex shapes. Although the 3D bio-printing technique provides channels with desired shapes, there are some drawbacks that hinder the application of this technique more easily. For example, printing large-size tissues with high resolution (less than 100 μm) using a 3D printer takes a long time; thus, the size or resolution of the tissues is limited by the printing time so as not to damage cells [121]. In contrast, the time it takes to fabricate the tissue using our technique is not much increased by the size of the desired tissues since our approach only requires a single instant injection by pipette, even for a larger structure. Additionally, the cell density of the printed tissues is usually lower than the physiological cell density (10-500 million cells/mL) because of the crosslinking solution of the inks and reducing shear stress in most inkjet bio-printing cases [98]. Since our technique can overcome these limitations and requires only two stainless pins with a gelatin solution, it could be used instead of a 3D printer when a straight vasculature is needed in engineered muscles with high cell density. This technique can also be broadly applied in the fields of tissue engineering and regenerative medicine by replacing the outer skeletal muscle layer with other organ cells.

Chapter 4

Conclusion

Although there is a growing demand for high-performance engineered skeletal muscle tissues (eSMTs) as drug testing platforms, implantable tissues, and actuators for a biological machine, their practical use has been delayed by the critical gap between *in vitro* and *in vivo* skeletal muscles' functionality and micro-structure. This thesis explored the two different ways to improve the functionalities and overcome the size limit of eSMTs inspired by nature of *in vivo* skeletal muscles: 1) training the eSMTs to manipulate their extracellular matrix (ECM) appropriately through application of alternating electrical and mechanical stimulation (chapter 2) and 2) creating perfusable vascular channel in the tissue and incorporating two separate media for each cell type to increase the size of eSMTs and to enhance contractile performance (chapter 3).

In chapter 2, the contractile force of eSMTs is improved by 20% in 3 minutes and 30% in 20 minutes through coordinated mechanical stretching and electric potential stimulation. The interactions between the myotubes and the surrounding ECM during the stimulation were investigated, and it was shown that the ECM fibers changed their orientations and thereby changed the stiffness of the ECM network as the alternating mechanical and electrical stimulation was applied. This ECM remodeling decreases the stiffness of the ECM network that is parallel to the myotubes so that the parallel ECM does not impede the muscle contraction. Furthermore, this ECM remodeling increases the stiffness of the ECM network that is serial to the myotubes, so that the

contractile force can be transmitted along a series of myotubes connected by the serial ECM. This is shown in chapter 2 by measuring the orientation distribution of collagen fibers to characterize the ECM remodeling induced by the coordinated stimulation. Moreover, a mechanistic model was proposed to better elucidate the effect of ECM remodeling upon the generation and transmission of the contractile force in eSMTs. This work sheds light on the difficulty of enhancing the contractile performance of eSMTs in two aspects. The first is the development of the novel training method using coordinated electric and mechanical stimulation, and the second is the discovery that ECM remodeling is heavily involved in this performance enhancement with the mechanistic model, allowing the myotubes to generate a higher contractile force and effectively transmit the force to the load.

In chapter 3, a novel platform to fabricate human eSMTs with a perfusable vascular channel is described to increase their size through the vasculature. Achieving muscle differentiation and growth of endothelial cells at the same time by coculturing myoblasts and endothelial cells has been challenging because of incompatible medium problem. By implementing the extracellular fluid compartments to the *in vitro* platform, the two separate media for each cell type were provided to eSMTs with direct contact between muscle and endothelial cells for their interactions. Using the two separate media led to significant enhancement of muscle contractile force with the formation of a vasculature simultaneously. Moreover, vascularized human eSMTs were constructed in various sizes of submillimeter to subcentimeter by forming the perfusable vascular channel in the eSMT. Experiments using the small-scale tissues as a model of human skeletal muscles uncovered the effects of coculture timing relative to muscle differentiation on the functionalities of the two cell types and the influence of vascularization on the responses to a myotoxic drug. The newly developed eSMTs with a physiological level of muscle cell density were further vascularized by inducing angiogenesis from the perfusable vasculature into the muscle tissue layer. Additionally, the prevascularized large-size eSMTs without using a synthetic membrane will be used as implantable tissues for treating volumetric muscle loss. Lastly, the ability to recapitulate the blood-organ barrier will be invaluable for vascularization of engi-

neered tissues, especially when cell culture conditions for host cells and endothelial cells are incompatible. We believe this promising methodology for scaling up eSMTs and improving their functionalities will open new opportunities in multidisciplinary fields, translational research, tissue engineering, and pharmacology.

Appendix A

Supplementary Figures for Chapter 2

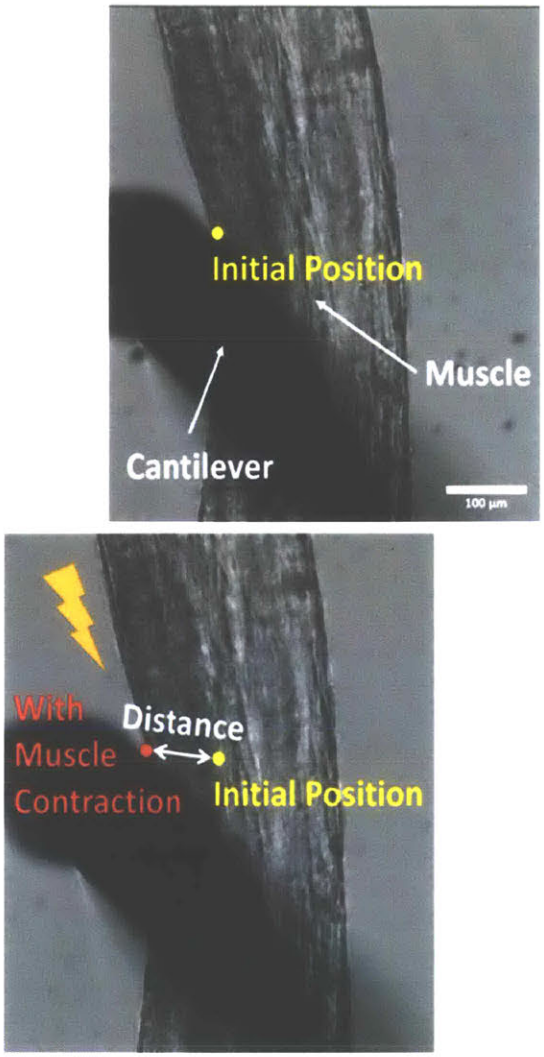

Figure A-1: Measurement of the muscle contractile force. These images are an enlargement of the contact point between the eSMT and the tip of cantilever in Fig. 2-1c during muscle contraction. The point of the force balance between the elastic force of the cantilever wire and the forces from the eSMT is shifted by inducing muscle contraction, and the moving distance of the cantilever is proportional to the contractile force. Yellow dot is original force equilibrium position, and the yellow dot is shifted to the red one by the contractile force.

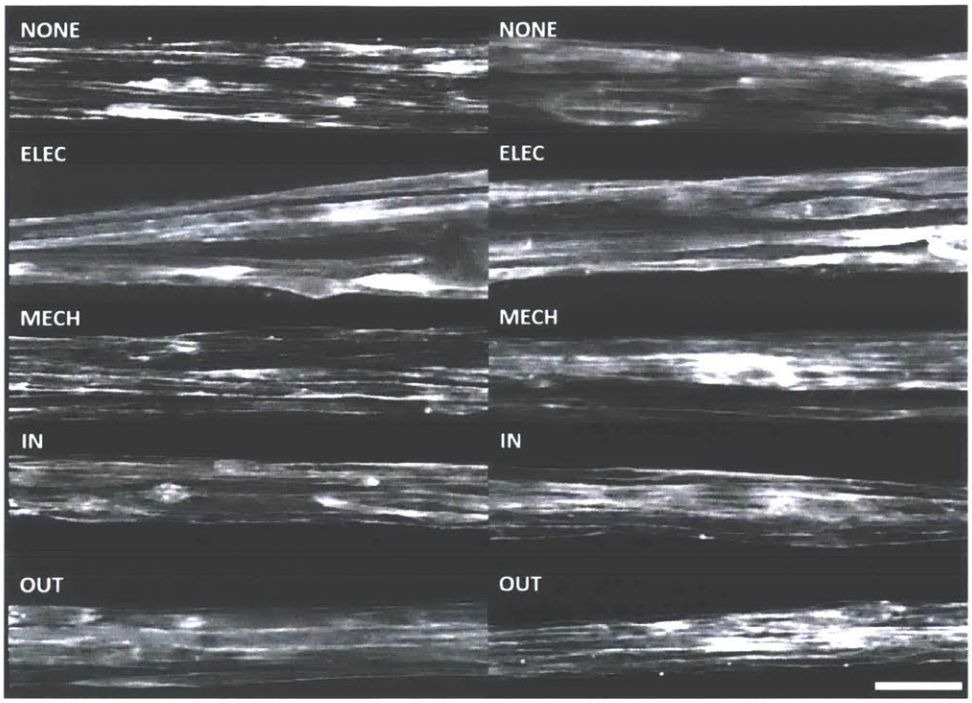

Figure A-2: Immunostaining images of actin in the eSMTs following the application of the electric potential (ELEC), mechanical stretching (MECH), in-phase co-stimulation (IN), and out-of-phase co-stimulation (OUT) for 3 minutes. There was no notable difference in the actin networks between the 3-minute stimulation conditions. Scale bar represents 100 μm.

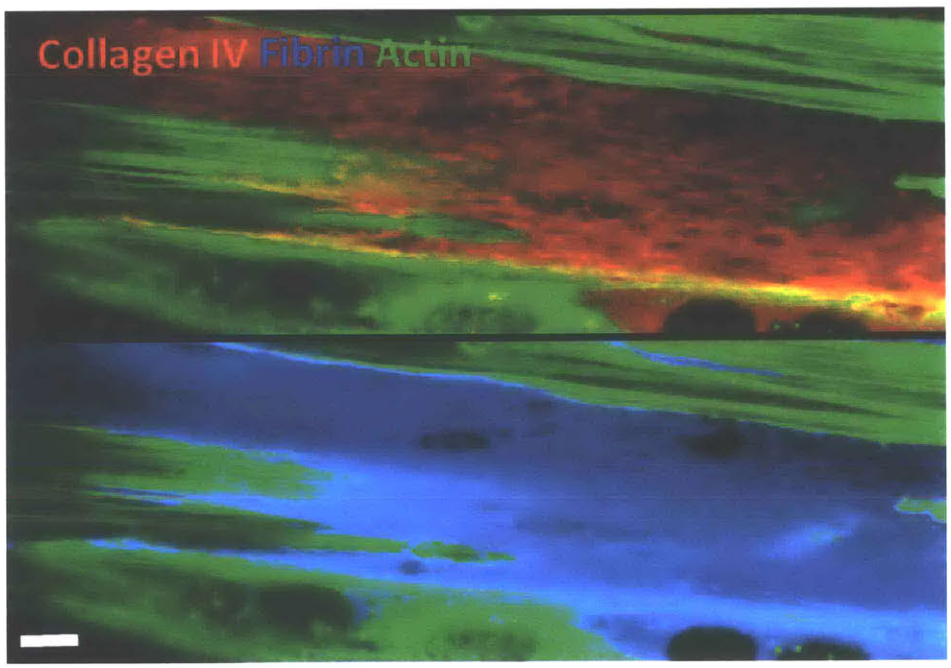

Figure A-3: Immunostaining images of collagen IV (red), fibrin (blue), and actin (green) in the unstimulated eSMT. Fibrin was much more aggregated than collagen IV. Scale bar represents 10 μm.

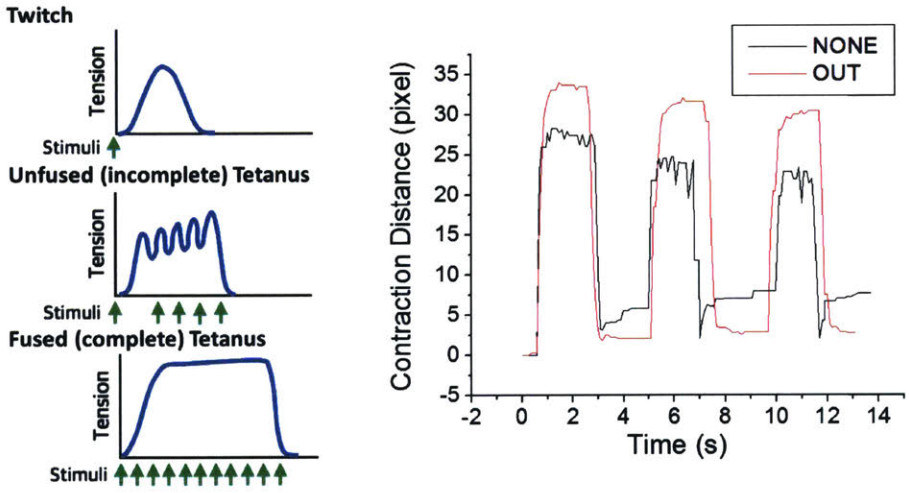

Figure A-4: An unfused tetanus of the untrained muscles became a fused tetanus by applying 3 minutes of the out-of-phase co-stimulation. (Left) The concept of the twitch, unfused tetanus and fused tetanus. In the general case of the native muscles, they show twitch, unfused or fused tetanus according to the frequency of the applied electrical stimulation. (Right) Although the stimulation frequency (2.5 V/mm, 1 ms, 60 Hz) was same, the unfused tetanus changed to the fused tetanus after applying the out-of-phase co-stimulation to the eSMT for 3 minutes.

Appendix B

Supplementary Figures for Chapter 3

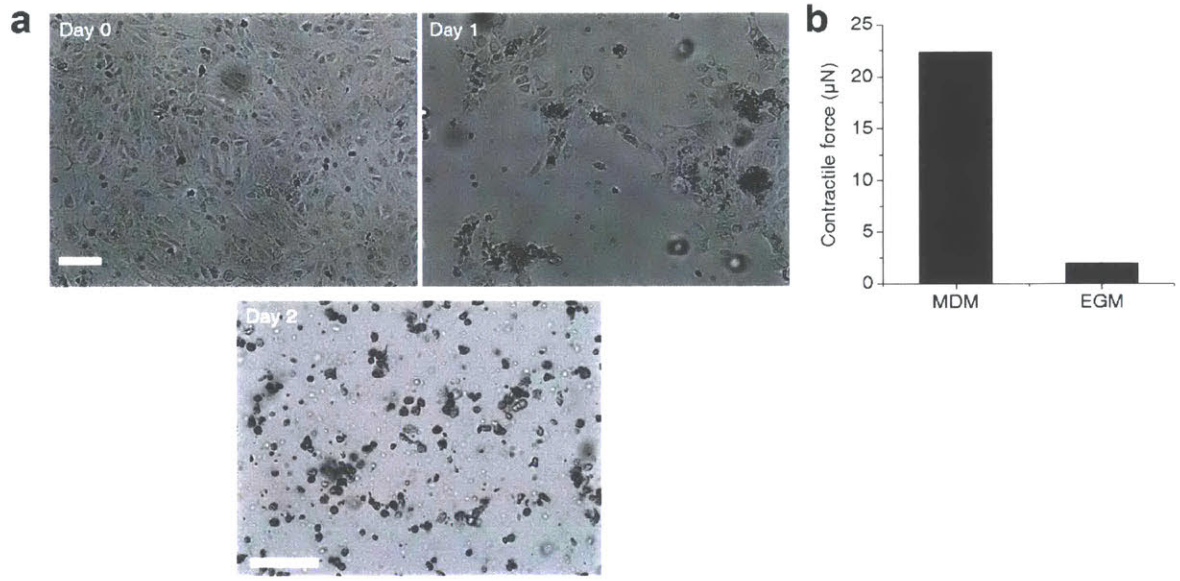

Figure B-1: Incompatible two cell culture media for endothelial cells and muscle cells. **a**. Images of endothelial cells on flasks cultured in muscle differentiation medium (MDM) on Day 0, 1, and 2. Scale bars represent 100 μm. **b**. Contractile force of the three-dimensional engineered skeletal muscle tissues on Day 8 cultured in MDM and endothelial cell growth medium (EGM).

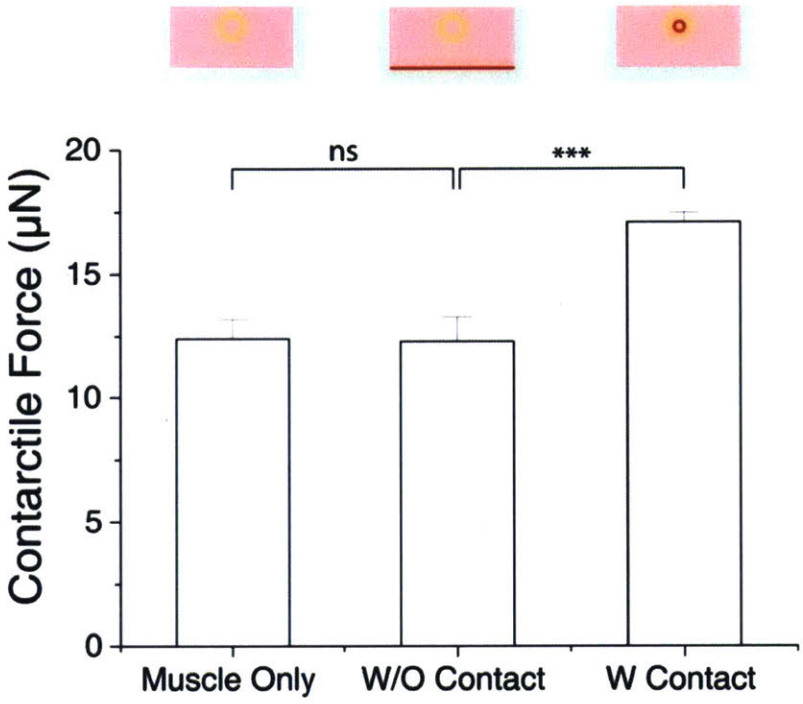

Figure B-2: The effect of the contact between muscle cells (MCs) and endothelial cells (ECs) on the function of the engineered muscle tissues. The contractile forces of tissues in the conditions of MCs only (Muscle Only), MCs cultured with ECs without contact between the two cell types by seeding the ECs at the surface approximately 3 mm far from the muscle tissue (W/O Contact) or with the contact by seeding ECs in the inner channel of the muscle tissue (W Contact). The tissues with the contact (W Contact) produced the highest contractile force. SEM, n = 4, 5, and 9. $^{***}P < 0.001$ and ns, not significant.

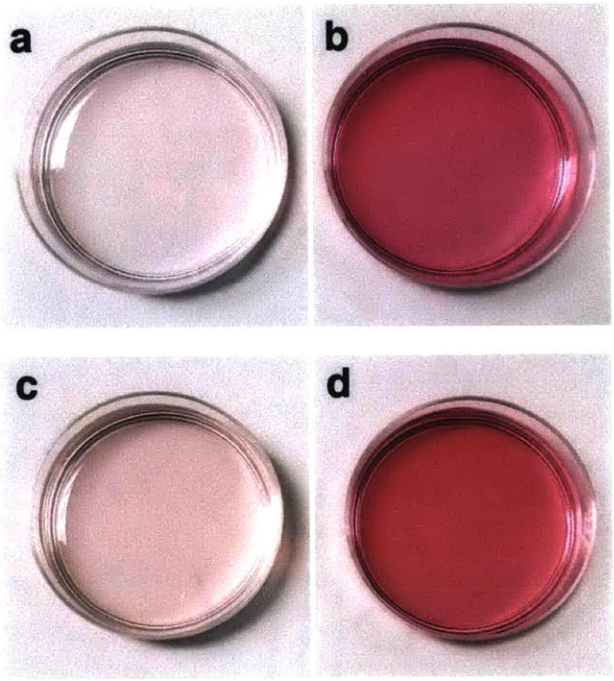

Figure B-3: Tubular vascularized muscle tissues were incubated with the endothelial cell growth medium (EGM) and the muscle differentiation medium (MDM) in the inner channel and the outer medium space for one day, and the two differently colored liquids were not mixed. **a**, **b**. Fresh EGM (**a**) and MDM (**b**). **c**, **d**. Conditioned EGM (**c**) and MDM (**d**) that were incubated with the vascularized muscle tissue for 24 hours.

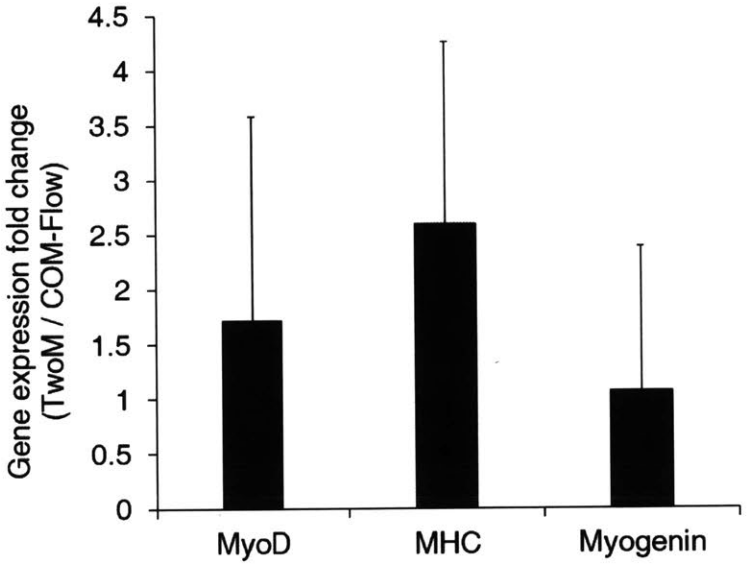

Figure B-4: Relative mRNA expression (the two separate medium over the single co-culture medium with flow) of the muscle differentiation markers (MyoD, myosin heavy chain (MHC), and Myogenin). SD, n = all 3. TwoM: the two separate medium, COM-Flow: the single co-culture medium with flow.

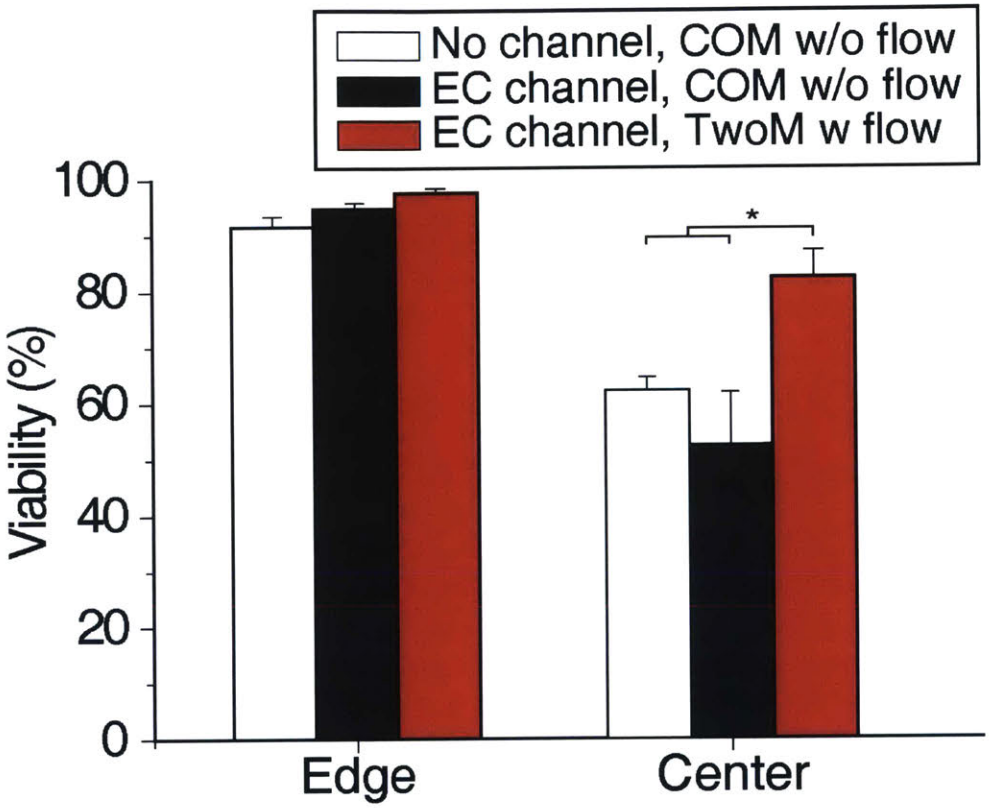

Figure B-5: Culturing the engineered skeletal muscle tissues in the TwoM using the vascular channel (EC channel) enhanced viability of the cells at the center part of the large-size tissue compared to the eSMTs without the channel and with the vascular channel cultured in the COM without a flow. SEM. n = 3, 4, 4, 2, 3, and 3. ANOVA with Tukey post-test. $^*P < 0.05$

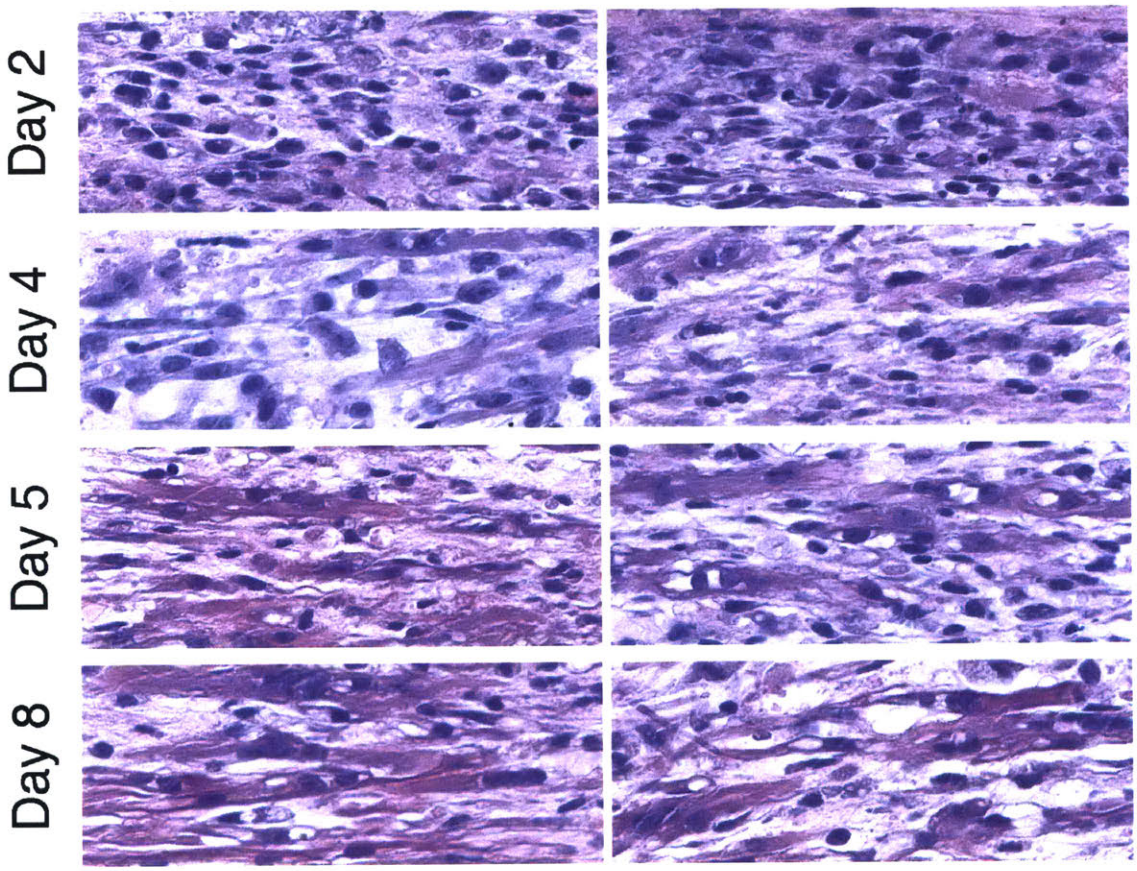

Figure B-6: Hematoxylin-eosin (H&E) staining of longitudinal sections of the eSMTs at Day 2, 4, 5, and 8 from the eSMT formation in the co-culture medium to measure the fusion rate over time.

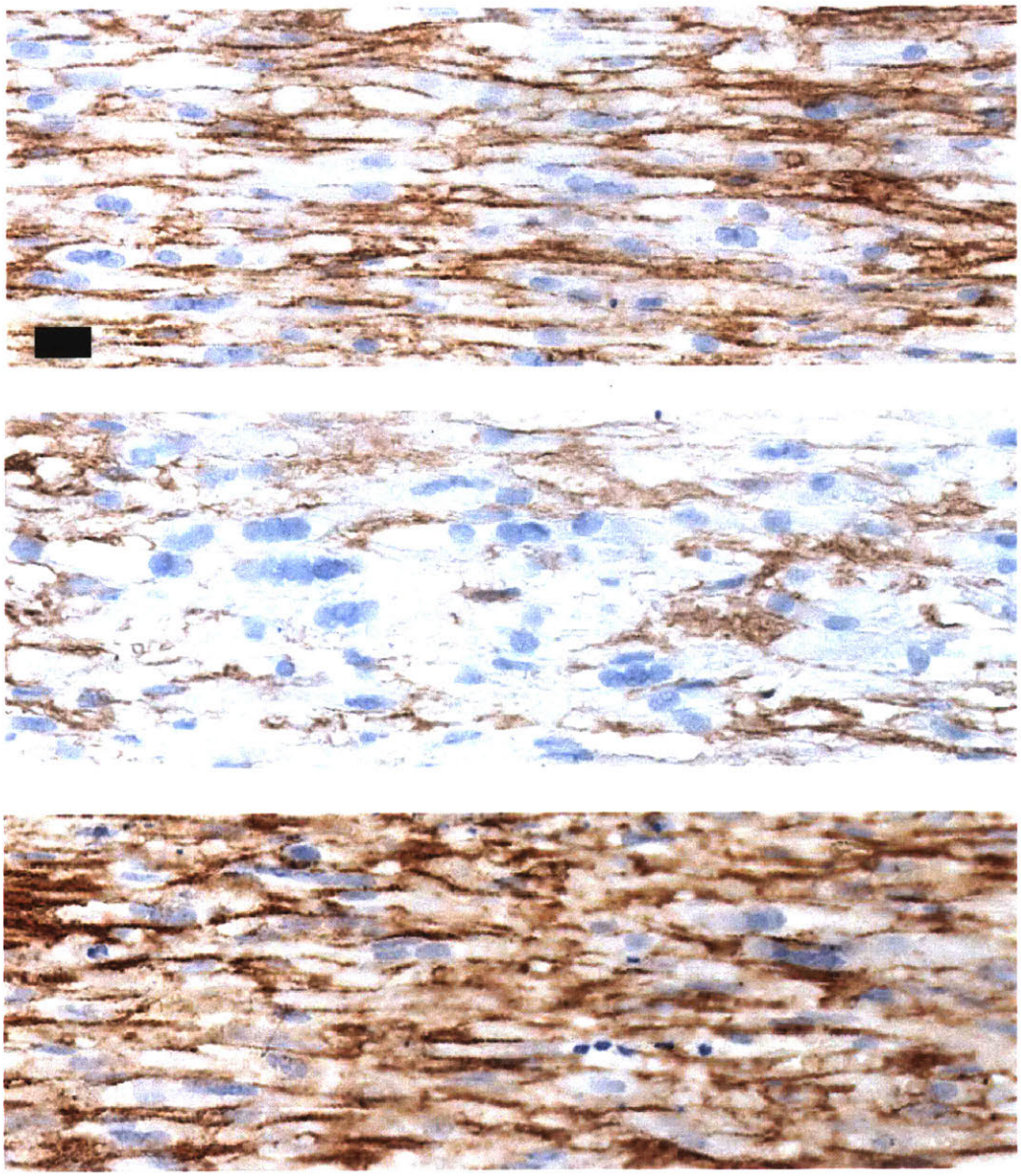

Figure B-7: Histological sectioned images of the muscle tissues in the conditions of the muscle only (top), co-culture from day 2 (middle) or day 5 (bottom) of muscle tissue fabrication show myotube thickness and cell alignment in the longitudinal direction of the tissue. Laminin and nucleus were stained in brown and blue, respectively. Scale bar is 10 μm.

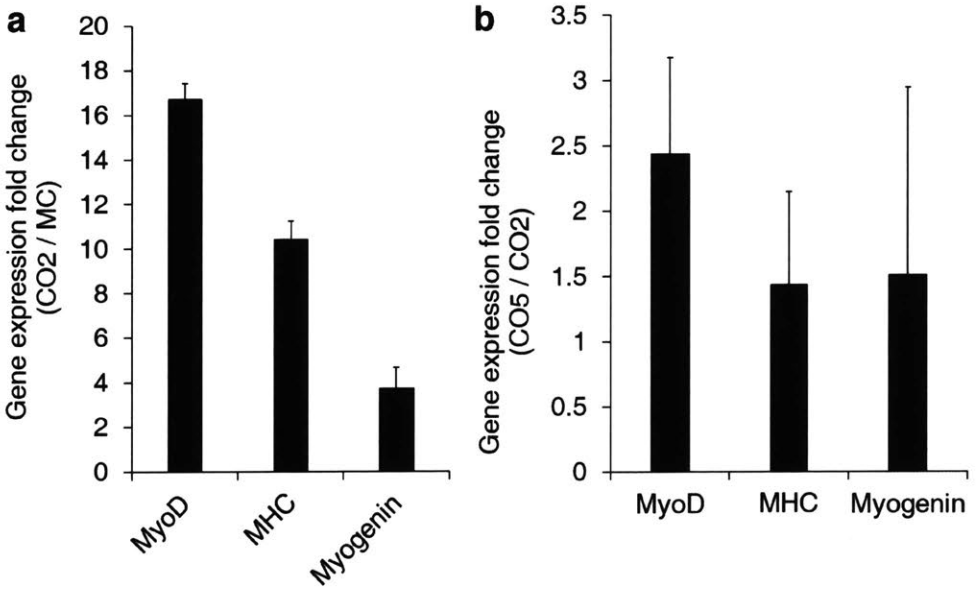

Figure B-8: Relative mRNA expression of the muscle differentiation markers (MyoD, myosin heavy chain (MHC), and Myogenin). **a**. mRNA expression of the condition of seeding the endothelial cells at day 2 of tissue fabrication (CO2) relative to the muscle-only condition (MC). SD, n = all 3. **b**. mRNA expression of the condition of seeding the endothelial cells at day 5 of tissue fabrication (CO5) relative to the CO2 condition (MC). SD, n = all 3.

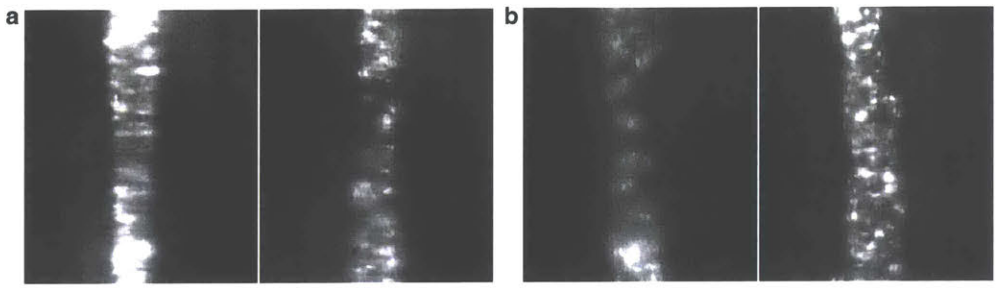

Figure B-9: In the conditions of the co-culture from day 2 (**a**) or day 5 (**b**) of muscle tissue fabrication, the RFP-human umbilical vein endothelial cells that seeded in the inner channel of the tubular muscle tissue stayed in the inner channel, instead of sprouting into the muscle tissue.

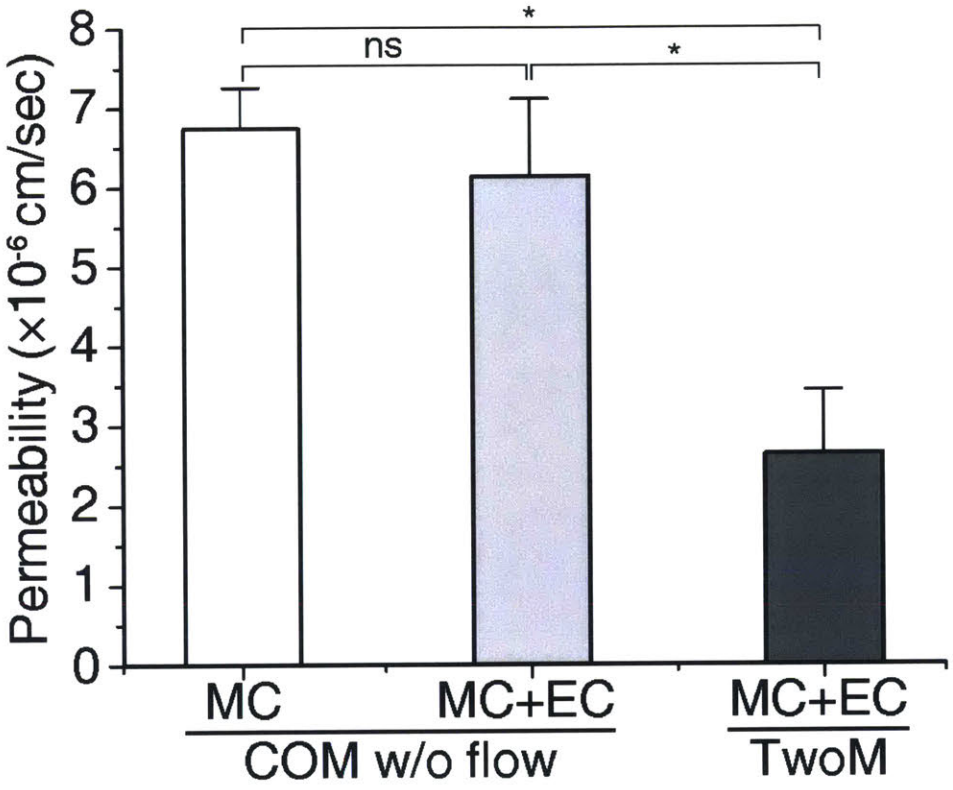

Figure B-10: Permeability of the inner channel in the conditions of muscle only (MC) and co-culture (MC+EC) in the COM without flow and co-culture (MC+EC) in the TwoM with flow. SEM. n = all 4. ANOVA with Tukey post-test. $^*P < 0.05$ and ns, not significant.

Bibliography

[1] Devin Neal, Mahmut Selman Sakar, Rashid Bashir, Vincent Chan, and Haruhiko Harry Asada. Mechanical characterization and shape optimization of fascicle-like 3D skeletal muscle tissues contracted with electrical and optical stimuli. *Tissue Eng. Part A*, 21(11-12):1848–1858, 2015.

[2] Gaurav Agrawal, Aereas Aung, and Shyni Varghese. Skeletal muscle-on-a-chip: An in vitro model to evaluate tissue formation and injury. *Lab Chip*, 17:3447–3461, sep 2017.

[3] Alec S.T. Smith, Jennifer Davis, Gabsang Lee, David L. Mack, and Deok-Ho Kim. Muscular dystrophy in a dish: engineered human skeletal muscle mimetics for disease modeling and drug discovery. *Drug Discovery Today*, 21(9):1387 – 1398, 2016.

[4] Eric W Esch, Anthony Bahinski, and Dongeun Huh. Organs-on-chips at the frontiers of drug discovery. *Nature Reviews Drug Discovery*, 14:248, mar 2015.

[5] Linda G Griffith and Melody A Swartz. Capturing complex 3d tissue physiology in vitro. *Nat. Rev. Mol. Cell Biol.*, 7(3):211, 2006.

[6] Junhee Seok, H Shaw Warren, Alex G Cuenca, Michael N Mindrinos, Henry V Baker, Weihong Xu, Daniel R Richards, Grace P McDonald-Smith, Hong Gao, Laura Hennessy, et al. Genomic responses in mouse models poorly mimic human inflammatory diseases. *Proc. Natl. Acad. Sci.*, 110(9):3507–3512, 2013.

[7] Dongeun Huh, Geraldine A. Hamilton, and Donald E. Ingber. From 3d cell culture to organs-on-chips. *Trends Cell Biol.*, 21(12):745 – 754, 2011.

[8] Benjamin T. Corona, Catherine L. Ward, Hannah B. Baker, Thomas J. Walters, and George J. Christ. Implantation of in vitro tissue engineered muscle repair constructs and bladder acellular matrices partially restore in vivo skeletal muscle function in a rat model of volumetric muscle loss injury. *Tissue Engineering Part A*, 20(3-4):705–715, 2014.

[9] Hee Seok Yang, Nicholas Ieronimakis, Jonathan H. Tsui, Hong Nam Kim, Kahp-Yang Suh, Morayma Reyes, and Deok-Ho Kim. Nanopatterned muscle cell patches for enhanced myogenesis and dystrophin expression in a mouse model of muscular dystrophy. *Biomaterials*, 35(5):1478 – 1486, 2014.

[10] Giorgio Cittadella Vigodarzere and Sara Mantero. Skeletal muscle tissue engineering: strategies for volumetric constructs. *Frontiers in Physiology*, 5:362, sep 2014.

[11] Paola Spitalieri, Valentina Rosa Talarico, Michela Murdocca, Giuseppe Novelli, and Federica Sangiuolo. Human induced pluripotent stem cells for monogenic disease modelling and therapy. *World J. Stem Cells*, 8(4):118, 2016.

[12] Vincent Chan, Kidong Park, Mitchell B Collens, Hyunjoon Kong, Taher A Saif, and Rashid Bashir. Development of miniaturized walking biological machines. *Scientific Reports*, 2:857, nov 2012.

[13] Yuya Morimoto, Hiroaki Onoe, and Shoji Takeuchi. Biohybrid robot powered by an antagonistic pair of skeletal muscle tissues. *Science Robotics*, 3(18):eaat4440, 2018.

[14] Caroline Cvetkovic, Meghan C Ferrall-Fairbanks, Eunkyung Ko, Lauren Grant, Hyunjoon Kong, Manu O Platt, and Rashid Bashir. Investigating the life expectancy and proteolytic degradation of engineered skeletal muscle biological machines. *Scientific Reports*, 7(1):3775, 2017.

[15] Richard C Strohman, Ellen Bayne, Dennis Spector, Takashi Obinata, Julie Micou-Eastwood, and Andrew Maniotis. Myogenesis and histogenesis of skeletal muscle on flexible membranes in vitro. *In Vitro Cell Dev. Biol.*, 26(2):201–208, 1990.

[16] Robert G. Dennis, II Kosnik, Paul E., Mark E. Gilbert, and John A. Faulkner. Excitability and contractility of skeletal muscle engineered from primary cultures and cell lines. *Am. J. Physiol. Cell Physiol.*, 280(2):C288–295, feb 2001.

[17] H H Vandenburgh, S Swasdison, and P Karlisch. Computer-aided mechanogenesis of skeletal muscle organs from single cells in vitro. *FASEB J.*, 5(13):2860–2867, 1991.

[18] Mai T. Lam, Yen-Chih Huang, Ravi K. Birla, and Shuichi Takayama. Microfeature guided skeletal muscle tissue engineering for highly organized 3-dimensional free-standing constructs. *Biomaterials*, 30(6):1150 – 1155, 2009.

[19] Takahisa Okano, Shinichi Satoh, Takahiro Oka, and Takehisa Matsuda. Tissue engineering of skeletal muscle. highly dense, highly oriented hybrid muscular tissues biomimicking native tissues. *ASAIO J.*, 43(5):M749–53, 1997.

[20] Weining Bian, Brian Liau, Nima Badie, and Nenad Bursac. Mesoscopic hydrogel molding to control the 3d geometry of bioartificial muscle tissues. *Nat. Protoc.*, 4(10):1522, 2009.

[21] Yasunori Yamamoto, Akira Ito, Masahiro Kato, Yoshinori Kawabe, Kazunori Shimizu, Hideaki Fujita, Eiji Nagamori, and Masamichi Kamihira. Preparation

of artificial skeletal muscle tissues by a magnetic force-based tissue engineering technique. *J. Biosci. Bioeng.*, 108(6):538 - 543, 2009.

[22] Shulamit Levenberg, Jeroen Rouwkema, Mara Macdonald, Evan S Garfein, Daniel S Kohane, Diane C Darland, Robert Marini, Clemens A van Blitterswijk, Richard C Mulligan, Patricia A D'Amore, and Robert Langer. Engineering vascularized skeletal muscle tissue. *Nat. Biotechnol.*, 23:879, jun 2005.

[23] Amulya K Saxena, Jennifer Marler, Mark Benvenuto, Gunter H Willital, and Joseph P Vacanti. Skeletal muscle tissue engineering using isolated myoblasts on synthetic biodegradable polymers: preliminary studies. *Tissue Eng.*, 5(6):525–531, 1999.

[24] Janet Shansky, Joseph Chromiak, Michael Del Tatto, and Herman Vandenburgh. A simplified method for tissue engineering skeletal muscle organoids in vitro. *In Vitro Cell. Dev. Biol.*, 33(9):659–661, Sep 1997.

[25] Mark Juhas, George C. Engelmayr, Andrew N. Fontanella, Gregory M. Palmer, and Nenad Bursac. Biomimetic engineered muscle with capacity for vascular integration and functional maturation in vivo. *Proc. Natl. Acad. Sci.*, 111(15):5508–5513, 2014.

[26] Herman Vandenburgh, Janet Shansky, Frank Benesch-Lee, Victoria Barbata, Jonathan Reid, Lieven Thorrez, Robert Valentini, and Gregory Crawford. Drug-screening platform based on the contractility of tissue-engineered muscle. *Muscle Nerve*, 37(4):438–447, 2008.

[27] Devin Neal, Mahmut Selman Sakar, Lee-Ling S Ong, and H Harry Asada. Formation of elongated fascicle-inspired 3D tissues consisting of high-density, aligned cells using sacrificial outer molding. *Lab Chip*, 14(11):1907–1916, 2014.

[28] Hideaki Fujita, Kazunori Shimizu, Yasunori Yamamoto, Akira Ito, Masamichi Kamihira, and Eiji Nagamori. Fabrication of scaffold-free contractile skeletal muscle tissue using magnetite-incorporated myogenic c2c12 cells. *J. Tissue Eng. Regener. Med.*, 4(6):437–443, 2010.

[29] Yasunori Yamamoto, Akira Ito, Hideaki Fujita, Eiji Nagamori, Yoshinori Kawabe, and Masamichi Kamihira. Functional evaluation of artificial skeletal muscle tissue constructs fabricated by a magnetic force-based tissue engineering technique. *Tissue Eng., Part A*, 17(1-2):107–114, 2010.

[30] Herman Vandenburgh, Janet Shansky, Frank Benesch-Lee, Kirsten Skelly, Janelle M. Spinazzola, Yero Saponjian, and Brian S. Tseng. Automated drug screening with contractile muscle tissue engineered from dystrophic myoblasts. *FASEB J.*, 23(10):3325–3334, 2009.

[31] Weining Bian and Nenad Bursac. Tissue engineering of functional skeletal muscle: challenges and recent advances. *IEEE Eng. Med. Biol. Mag.*, 27(5):109–113, 2008.

[32] Richard L Lieber and Samuel R Ward. Skeletal muscle design to meet functional demands. *Philos. Trans. R. Soc. B Biol. Sci.*, 366(1570):1466–1476, may 2011.

[33] Hyeonyu Kim, Min-Cheol Kim, and H Harry Asada. Extracellular matrix remodelling induced by alternating electrical and mechanical stimulations increases the contraction of engineered skeletal muscle tissues. *Sci. Rep.*, 9(1):2732, 2019.

[34] J. Stern-Straeter, A.D. Bach, L. Stangenberg, V.T. Foerster, R.E. Horch, G.B. Stark, and J.P. Beier. Impact of electrical stimulation on three-dimensional myoblast cultures - a real-time RT-PCR study. *J. Cell. Mol. Med.*, 9(4):883–892, oct 2005.

[35] V Mudera, A S T Smith, M A Brady, and M P Lewis. The effect of cell density on the maturation and contractile ability of muscle derived cells in a 3D tissue-engineered skeletal muscle model and determination of the cellular and mechanical stimuli required for the synthesis of a postural phenotype. *J. Cell. Physio.*, 225(3):646–53, nov 2010.

[36] Quinlyn A Soltow, Elizabeth H Zeanah, Vitor A Lira, and David S Criswell. Cessation of cyclic stretch induces atrophy of C2C12 myotubes. *Biochem. Biophys. Res. Commun.*, 434(2):316–321, may 2013.

[37] Akira Ito, Yasunori Yamamoto, Masanori Sato, Kazushi Ikeda, Masahiro Yamamoto, Hideaki Fujita, Eiji Nagamori, Yoshinori Kawabe, and Masamichi Kamihira. Induction of functional tissue-engineered skeletal muscle constructs by defined electrical stimulation. *Sci. Rep.*, 4:4781, apr 2014.

[38] Cindy S Cheng, Brittany NJ Davis, Lauran Madden, Nenad Bursac, and George A Truskey. Physiology and metabolism of tissue-engineered skeletal muscle. *Exp. Biol. Med.*, 239(9):1203–1214, 2014.

[39] Peter P. Purslow. Muscle fascia and force transmission. *J. Bodyw. Mov. Ther.*, 14(4):411–417, oct 2010.

[40] Allison R Gillies and Richard L Lieber. Structure and function of the skeletal muscle extracellular matrix. *Muscle Nerve*, 44(3):318–331, sep 2011.

[41] Mohamed I Elashry, Henry Collins-Hooper, Sakthivel Vaiyapuri, and Ketan Patel. Characterisation of connective tissue from the hypertrophic skeletal muscle of myostatin null mice. *Journal of Anatomy*, 220(6):603–611, jun 2012.

[42] Angela K Peter, Hongqiang Cheng, Robert S Ross, Kirk U Knowlton, and Ju Chen. The costamere bridges sarcomeres to the sarcolemma in striated muscle. *Prog. Pediatr. Cardiol.*, 31(2):83–88, may 2011.

[43] Angelika C. Paul, Philip W. Sheard, Stephen J. Kaufman, and Marilyn J. Duxson. Localization of $\alpha 7$ integrins and dystrophin suggests potential for both

lateral and longitudinal transmission of tension in large mammalian muscles. *Cell Tissue Res.*, 308(2):255 265, 2002.

[44] Miriam Young, Angelika Paul, Judith Rodda, Marilyn Duxson, and Philip Sheard. Examination of intrafascicular muscle fiber terminations: Implications for tension delivery in series-fibered muscles. *J. Morphol.*, 245(2):130–145, 2000.

[45] Sandra Murphy, Margit Zweyer, Rustam R Mundegar, Michael Henry, Paula Meleady, Dieter Swandulla, and Kay Ohlendieck. Concurrent label-free mass spectrometric analysis of dystrophin isoform Dp427 and the myofibrosis marker collagen in crude extracts from mdx-4cv skeletal muscles. *Proteomes*, 3(3):298–327, 2015.

[46] Kelley M Virgilio, Kyle S Martin, Shayn M Peirce, and Silvia S Blemker. Multi-scale models of skeletal muscle reveal the complex effects of muscular dystrophy on tissue mechanics and damage susceptibility. *Interface Focus*, 5(2):20140080, feb 2015.

[47] Chi Zhang and Yingxin Gao. Finite element analysis of mechanics of lateral transmission of force in single muscle fiber. *J. Biomech.*, 45(11):2001–2006, jul 2012.

[48] MinCheol Kim, Jordan Whisler, Yaron R Silberberg, Roger D Kamm, and H Harry Asada. Cell invasion dynamics into a three dimensional extracellular matrix fibre network. *PLoS Comput. Biol.*, 11(10):e1004535, oct 2015.

[49] Peter P Purslow and John A Trotter. The morphology and mechanical properties of endomysium in series-fibred muscles: variations with muscle length. *J. Muscle Res. Cell Motil.*, 15(3):299–308, 1994.

[50] Yingxin Gao, Alan S Wineman, and Anthony M Waas. Time-dependent lateral transmission of force in skeletal muscle. *Proc. R. Soc. Lond. A Math. Phys. Sci.*, 465(2108):2441–2460, 2009.

[51] Godfrina McKoy, William Ashley, James Mander, Shi Yu Yang, Norman Williams, Brenda Russell, and Geoffrey Goldspink. Expression of insulin growth factor-1 splice variants and structural genes in rabbit skeletal muscle induced by stretch and stimulation. *J. Physiol.*, 516(2):583–592, apr 1999.

[52] G. Goldspink, A. Scutt, P. T. Loughna, D. J. Wells, T. Jaenicke, and G. F. Gerlach. Gene expression in skeletal muscle in response to stretch and force generation. *Am. J. Physiol. Regulatory Integrative Comp. Physiol.*, 262(3):R356–363, mar 1992.

[53] Pamela Williams, Peter Watt, V Bicik, and Geoffrey Goldspink. Effect of stretch combined with electrical stimulation on the type of sarcomeres produced at the ends of muscle fibers. *Exp. Neurol.*, 93(3):500–509, sep 1986.

[54] Andrea Pavesi, Giulia Adriani, Marco Rasponi, Ioannis K Zervantonakis, Gianfranco B Fiore, and Roger D Kamm. Controlled electromechanical cell stimulation on-a-chip. *Sci. Rep.*, 5:11800, jul 2015.

[55] Jia-Ling Ruan, Nathaniel L. Tulloch, Maria V. Razumova, Mark Saiget, Veronica Muskheli, Lil Pabon, Hans Reinecke, Michael Regnier, and Charles E. Murry. Mechanical stress conditioning and electrical stimulation promote contractility and force maturation of induced pluripotent stem cell-derived human cardiac tissue. *Circulation*, 134(20):1557–1567, 2016.

[56] Hyoungshin Park, Benjamin L Larson, Martin E Kolewe, Gordana Vunjak-Novakovic, and Lisa E Freed. Biomimetic scaffold combined with electrical stimulation and growth factor promotes tissue engineered cardiac development. *Exp. Cell Res.*, 321(2):297–306, feb 2014.

[57] I-Chien Liao, Jason B. Liu, Nenad Bursac, and Kam W. Leong. Effect of electromechanical stimulation on the maturation of myotubes on aligned electrospun fibers. *Cell Mol. Bioeng.*, 1(2):133–145, Sep 2008.

[58] J. Uhlendorf, A. Miermont, T. Delaveau, G. Charvin, F. Fages, S. Bottani, G. Batt, and P. Hersen. Long-term model predictive control of gene expression at the population and single-cell levels. *Proc. Natl. Acad. Sci.*, 109(35):14271–14276, aug 2012.

[59] R Rezakhaniha, A Agianniotis, J T C Schrauwen, A Griffa, D Sage, C V C Bouten, F N van de Vosse, M Unser, and N Stergiopulos. Experimental investigation of collagen waviness and orientation in the arterial adventitia using confocal laser scanning microscopy. *Biomech. Model Mechanobiol.*, 11(3):461–473, 2012.

[60] P R Cavanagh and P V Komi. Electromechanical delay in human skeletal muscle under concentric and eccentric contractions. *Eur. J. Appl. Physiol. Occup. Physiol.*, 42(3):159–163, 1979.

[61] Eduardo Ríos, Jianjie Ma, and Adom González. The mechanical hypothesis of excitation-contraction (EC) coupling in skeletal muscle. *J. Muscle Res. Cell Motil.*, 12(2):127–135, 1991.

[62] Courtney A Powell, Beth L Smiley, John Mills, and Herman H Vandenburgh. Mechanical stimulation improves tissue-engineered human skeletal muscle. *Am. J. Physiol. Cell Physiol.*, 283(5):C1557–65, nov 2002.

[63] Koji Sakiyama, Shinichi Abe, Yuichi Tamatsu, and Yoshinobu Ide. Effects of stretching stress on the muscle contraction proteins of skeletal muscle myoblasts. *Biomed. Res.*, 26(2):61–68, 2005.

[64] Takayuki Akimoto, Takashi Ushida, Shigeru Miyaki, Tetsuya Tateishi, and Toru Fukubayashi. Mechanical stretch is a down-regulatory signal for differentiation

of C2C12 myogenic cells. *Mater. Sci. Eng. C Mater. Biol. Appl.*, 17(1-2):75–78, nov 2001.

[65] Allison R Gillies and Richard L Lieber. Structure and function of the skeletal muscle extracellular matrix. *Muscle Nerve*, 44(3):318–31, sep 2011.

[66] N Light and A E Champion. Characterization of muscle epimysium, perimysium and endomysium collagens. *Biochem. J.*, 219(3):1017–1026, may 1984.

[67] Sandra Murphy and Kay Ohlendieck. *The extracellular matrix complexome from skeletal muscle.* InTech, 2016.

[68] Miranda D Grounds. Complexity of extracellular matrix and skeletal muscle regeneration. In Stefano Schiaffino and Terence Partridge, editors, *Skeletal muscle repair and regeneration*, pages 269–301. Springer Science & Business Media, 2008.

[69] Satu O A Koskinen, Michael Kjær, Thomas Mohr, Fin Biering Sørensen, Tiina Suuronen, and Timo E S Takala. Type IV collagen and its degradation in paralyzed human muscle: Effect of functional electrical stimulation. *Muscle Nerve*, 23(4):580–589, 2000.

[70] Gretchen A Meyer and Richard L Lieber. Elucidation of extracellular matrix mechanics from muscle fibers and fiber bundles. *J. Biomech.*, 44(4):771–773, feb 2011.

[71] K A P Edman. Contractile properties of mouse single muscle fibers, a comparison with amphibian muscle fibers. *J. Exp. Biol.*, 208(10):1905–1913, 2005.

[72] Sara Romanazzo, Giancarlo Forte, Mitsuhiro Ebara, Koichiro Uto, Stefania Pagliari, Takao Aoyagi, Enrico Traversa, and Akiyoshi Taniguchi. Substrate stiffness affects skeletal myoblast differentiation in vitro. *Sci. Technol. Adv. Mater.*, 13(6):64211, nov 2012.

[73] Christopher W Ward, Benjamin L Prosser, and W Jonathan Lederer. Mechanical stretch-induced activation of ROS/RNS signaling in striated muscle. *Antioxid Redox Signal.*, 20(6):929–936, 2014.

[74] Sheng-Lin Lee, Ali Nekouzadeh, Boyd Butler, Kenneth M Pryse, William B McConnaughey, Adam C Nathan, Wesley R Legant, Pascal M Schaefer, Robert B Pless, Elliot L Elson, and Guy M Genin. Physically-induced cytoskeleton remodeling of cells in three-dimensional culture. *PloS One*, 7(12):e45512, jan 2012.

[75] Li Zuo, Leonardo Nogueira, and Michael C Hogan. Reactive oxygen species formation during tetanic contractions in single isolated Xenopus myofibers. *J. Appl. Physiol.*, 111(3):898–904, sep 2011.

[76] C D Balnave and D G Allen. The effect of muscle length on intracellular calcium and force in single fibres from mouse skeletal muscle. *J. Physiol.*, 492(3):705–713, may 1996.

[77] Nobuaki Sasai, Nobuhide Agata, Masumi Inoue-Miyazu, Keisuke Kawakami, Kunihiko Kobayashi, Masahiro Sokabe, and Kimihide Hayakawa. Involvement of PI3K/Akt/TOR pathway in stretch-induced hypertrophy of myotubes. *Muscle Nerve*, 41(1):100–106, jan 2010.

[78] Quinlyn A Soltow, Vitor A Lira, Jenna L Betters, Jodi H D Long, Jeff E Sellman, Elizabeth H Zeanah, and David S Criswell. Nitric oxide regulates stretch-induced proliferation in C2C12 myoblasts. *J. Muscle Res. Cell Motil.*, 31(3):215–225, 2010.

[79] Maya Shamir, Yinon Bar-On, Rob Phillips, and Ron Milo. Snapshot: timescales in cell biology. *Cell*, 164(6):1302 – 1302.e1, 2016.

[80] Hironobu Takahashi, Tatsuya Shimizu, and Teruo Okano. Engineered Human Contractile Myofiber Sheets as a Platform for Studies of Skeletal Muscle Physiology. *Sci. Rep.*, 8(1):13932, 2018.

[81] Marco Quarta, Melinda Cromie, Robert Chacon, Justin Blonigan, Victor Garcia, Igor Akimenko, Mark Hamer, Patrick Paine, Merel Stok, Joseph B Shrager, and Thomas A Rando. Bioengineered constructs combined with exercise enhance stem cell-mediated treatment of volumetric muscle loss. *Nat. Commun.*, 8:15613, jun 2017.

[82] Ami R. Amini, Cato T. Laurencin, and Syam P. Nukavarapu. Bone tissue engineering: recent advances and challenges. *Critical Reviews™ in Biomedical Engineering*, 40(5):363–408, 2012.

[83] Mark Juhas, George C. Engelmayr, Andrew N. Fontanella, Gregory M. Palmer, and Nenad Bursac. Biomimetic engineered muscle with capacity for vascular integration and functional maturation in vivo. *Proc. Natl. Acad. Sci.*, 111(15):5508–5513, 2014.

[84] Milica Radisic, Liming Yang, Jan Boublik, Richard J. Cohen, Robert Langer, Lisa E. Freed, and Gordana Vunjak-Novakovic. Medium perfusion enables engineering of compact and contractile cardiac tissue. *Am. J. Physiol. Heart Circ. Physiol.*, 286(2):H507 – H516, 2004.

[85] Seema M Ehsan and Steven C George. Nonsteady state oxygen transport in engineered tissue: implications for design. *Tissue Eng. Part A*, 19(11-12):1433–1442, jun 2013.

[86] Matthias W. Laschke and Michael D. Menger. Prevascularization in tissue engineering: Current concepts and future directions. *Biotechnol. Adv.*, 34(2):112 – 121, 2016.

[87] Michael Lovett, Kyongbum Lee, Aurelie Edwards, and David L Kaplan. Vascularization strategies for tissue engineering. *Tissue Eng. Part B Rev.*, 15(3):353–370, sep 2009.

[88] Tatsuya Osaki, Vivek Sivathanu, and Roger D. Kamm. Crosstalk between developing vasculature and optogenetically engineered skeletal muscle improves muscle contraction and angiogenesis. *Biomaterials*, 156:65 – 76, 2018.

[89] Joseph M. McClung, Jessica L. Reinardy, Sarah B. Mueller, Timothy J. McCord, Christopher D. Kontos, David A. Brown, Sabah N. A. Hussain, Cameron A. Schmidt, Terence E. Ryan, and Tom D. Green. Muscle cell derived angiopoietin-1 contributes to both myogenesis and angiogenesis in the ischemic environment. *Front. Physiol.*, 6:161, 2015.

[90] Cindy S Cheng, Yasser El-Abd, Khanh Bui, Young-Eun Hyun, Rebecca Harbuck Hughes, William E Kraus, and George A Truskey. Conditions that promote primary human skeletal myoblast culture and muscle differentiation in vitro. *Am. J. Physiol. Cell Physiol.*, 306(4):C385 C395, feb 2014.

[91] Dan H. Moore. Spesies differences in serum protein patterns. *J. Biol. Chem.*, 161(1):21 32, nov 1945.

[92] Jana Franke, Vanessa Abs, Claudia Zizzadoro, and Getu Abraham. Comparative study of the effects of fetal bovine serum versus horse serum on growth and differentiation of primary equine bronchial fibroblasts. *BMC Vet. Res.*, 10(1):119, May 2014.

[93] Dacha Gholobova, Lieselot Decroix, Vicky Van Muylder, Linda Desender, Melanie Gerard, Gilles Carpentier, Herman Vandenburgh, and Lieven Thorrez. Endothelial network formation within human tissue-engineered skeletal muscle. *Tissue Eng. Part A.*, 21(19-20):2548–2558, 2015.

[94] Sara Martina Maffioletti, Shilpita Sarcar, Alexander B H Henderson, Ingra Mannhardt, Luca Pinton, Louise Anne Moyle, Heather Steele-Stallard, Ornella Cappellari, Kim E Wells, Giulia Ferrari, Jamie S Mitchell, Giulia E Tyzack, Vassilios N Kotiadis, Moustafa Khedr, Martina Ragazzi, Weixin Wang, Michael R Duchen, Rickie Patani, Peter S Zammit, Dominic J Wells, Thomas Eschenhagen, and Francesco Saverio Tedesco. Three-dimensional human ipsc-derived artificial skeletal muscles model muscular dystrophies and enable multilineage tissue engineering. *Cell Rep.*, 23(3):899–908, apr 2018.

[95] Mikaela SjÃűstrand, Agneta HolmÃďng, and Peter LÃűnnroth. Measurement of interstitial insulin in human muscle. *Am. J. Physiol. Endocrinol. Metab.*, 276(1):E151 E154, 1999.

[96] Simone Bersini, Mara Gilardi, Giovanni S. Ugolini, Veronica Sansoni, Giuseppe TalÃš, Silvia Perego, Simona Zanotti, Paola Ostano, Marina Mora, Monica Soncini, Marco Vanoni, Giovanni Lombardi, and Matteo Moretti. Engineering

an environment for the study of fibrosis: a 3d human muscle model with endothelium specificity and endomysium. *Cell Rep.*, 25(13):3858 – 3868.e4, 2018.

[97] Jessie S. Jeon, Simone Bersini, Mara Gilardi, Gabriele Dubini, Joseph L. Charest, Matteo Moretti, and Roger D. Kamm. Human 3d vascularized organotypic microfluidic assays to study breast cancer cell extravasation. *Proc. Natl. Acad. Sci.*, 112(1):214–219, 2015.

[98] Sean V Murphy and Anthony Atala. 3d bioprinting of tissues and organs. *Nat. Biotechnol.*, 32:773, aug 2014.

[99] Ji Hyun Kim, Young-Joon Seol, In Kap Ko, Hyun-Wook Kang, Young Koo Lee, James J Yoo, Anthony Atala, and Sang Jin Lee. 3D bioprinted human skeletal muscle constructs for muscle function restoration. *Sci. Rep.*, 8(1):12307, 2018.

[100] Dongeun Huh, Benjamin D. Matthews, Akiko Mammoto, Martín Montoya-Zavala, Hong Yuan Hsin, and Donald E. Ingber. Reconstituting organ-level lung functions on a chip. *Science*, 328(5986):1662–1668, 2010.

[101] Magdalena Kasendra, Alessio Tovaglieri, Alexandra Sontheimer-Phelps, Sasan Jalili-Firoozinezhad, Amir Bein, Angeliki Chalkiadaki, William Scholl, Cheng Zhang, Hannah Rickner, Camilla A Richmond, Hu Li, David T Breault, and Donald E Ingber. Development of a primary human small intestine-on-a-chip using biopsy-derived organoids. *Sci. Rep.*, 8(1):2871, 2018.

[102] Ji Hoon Kim, Yixin Ren, Win Pin Ng, Shuo Li, Sungmin Son, Yee-Seir Kee, Shiliang Zhang, Guofeng Zhang, Daniel A. Fletcher, Douglas N. Robinson, and Elizabeth H. Chen. Mechanical tension drives cell membrane fusion. *Dev. Cell*, 32(5):561 – 573, 2015.

[103] J M Venuti, J H Morris, J L Vivian, E N Olson, and W H Klein. Myogenin is required for late but not early aspects of myogenesis during mouse development. *J. Cell Biol.*, 128(4):563–576, 1995.

[104] Paul D. Thompson, Priscilla Clarkson, and Richard H. Karas. Statin-Associated Myopathy. *J. Am. Med. Assoc.*, 289(13):1681–1690, 04 2003.

[105] Giuseppe Danilo Norata, Gianpaolo Tibolla, and Alberico Luigi Catapano. Statins and skeletal muscles toxicity: From clinical trials to everyday practice. *Pharmacol. Res.*, 88:107 – 113, 2014. Statin: New Life for an Old Drug.

[106] Ine Blankenberg Skottheim, Ane Gedde-Dahl, Solmaz Hejazifar, Kjersti Hoel, and Anders ÃĔsberg. Statin induced myotoxicity: The lactone forms are more potent than the acid forms in human skeletal muscle cells in vitro. *Eur. J Pharm. Sci.*, 33(4):317 – 325, 2008.

[107] K Korybalska, E Kawka, A Breborowicz, and J Witowski. Atorvastatin does not impair endothelial cell wound healing in an in vitro model of vascular injury. *J. Physiol. Pharmacol.*, 63(4):389–395, aug 2012.

[108] Li Wei, Jin-Shuen Chen, Hsin-Ting Lin, Chung-Ze Wu, Cai-Mei Zheng, Yu-Ching Chang, Li-Chien Chang, and Yuh-Feng Lin. Atorvastatin from target screening attenuates endothelial cell tube formation and migration by regulating urokinase receptor-related signaling pathway and f/g actin. *J. Chin. Med. Assoc.*, 80(2):86 – 95, 2017.

[109] Cédric Pisani, Estelle Rascol, Christophe Dorandeu, Jean-Charles Gaillard, Clarence Charnay, Yannick Guari, Joël Chopineau, Jean Armengaud, Jean-Marie Devoisselle, and Odette Prat. The species origin of the serum in the culture medium influences the in vitro toxicity of silica nanoparticles to HepG2 cells. *PloS one*, 12(8):e0182906–e0182906, aug 2017.

[110] L. Hermansen and M. Wachtlova. Capillary density of skeletal muscle in well-trained and untrained men. *J. Appl. Physiol.*, 30(6):860–863, 1971.

[111] Geraldine M. Mitchell and Wayne A. Morrison. *In Vitro and In Vivo Approaches for Pre-vascularization of 3-Dimensional Engineered Tissues*, pages 1–27. Vascularization for Tissue Engineering and Regenerative Medicine. Springer International Publishing, Cham, 2017.

[112] Bruno Vailhé, Daniel Vittet, and Jean-Jacques Feige. In Vitro Models of Vasculogenesis and Angiogenesis. *Lab. Invest.*, 81(4):439–452, 2001.

[113] Tara L. Haas and Emmanuel Nwadozi. Regulation of skeletal muscle capillary growth in exercise and disease. *Appl. Physiol. Nutr. Metab.*, 40(12):1221–1232, 2015.

[114] Geerten P. van Nieuw Amerongen, Pieter Koolwijk, Amanda Versteilen, and Victor W.M. van Hinsbergh. Involvement of rhoa/rho kinase signaling in vegf-induced endothelial cell migration and angiogenesis in vitro. *Arterioscler Thromb Vasc Biol.*, 23(2):211–217, 2003.

[115] Sachiko Sekiya, Tatsuya Shimizu, Masayuki Yamato, Akihiko Kikuchi, and Teruo Okano. Bioengineered cardiac cell sheet grafts have intrinsic angiogenic potential. *Biochem. Biophys. Res. Commun.*, 341(2):573 – 582, 2006.

[116] Fergal J. O'Brien. Biomaterials & scaffolds for tissue engineering. *Mater. Today*, 14(3):88 – 95, 2011.

[117] Serge Ostrovidov, Vahid Hosseini, Samad Ahadian, Toshinori Fujie, Selvakumar Prakash Parthiban, Murugan Ramalingam, Hojae Bae, Hirokazu Kaji, and Ali Khademhosseini. Skeletal muscle tissue engineering: methods to form skeletal myotubes and their applications. *Tissue Eng. Part B Rev.*, 20(5):403–436, oct 2014.

[118] Luba Perry, Shira Landau, Moshe Y Flugelman, and Shulamit Levenberg. Genetically engineered human muscle transplant enhances murine host neovascularization and myogenesis. *Commun Biol.*, 1(1):161, 2018.

[119] Jacob Koffler, Keren Kaufman-Francis, Yulia Shandalov, Dana Egozi, Daria Amiad Pavlov, Amir Landesberg, and Shulamit Levenberg. Improved vascular organization enhances functional integration of engineered skeletal muscle grafts. *Proc. Natl. Acad. Sci.*, 108(36):14789–14794, 2011.

[120] D Gholobova, M Gerard, L Decroix, L Desender, N Callewaert, P Annaert, and L Thorrez. Human tissue-engineered skeletal muscle: a novel 3D in vitro model for drug disposition and toxicity after intramuscular injection. *Sci. Rep.*, 8(1):12206, 2018.

[121] Yu Zhao, Yang Li, Shuangshuang Mao, Wei Sun, and Rui Yao. The influence of printing parameters on cell survival rate and printability in microextrusion-based 3D cell printing technology. *Biofabrication*, 7(4):045002, nov 2015.

[122] William J Polacheck, Matthew L Kutys, Jinling Yang, Jeroen Eyckmans, Yinyu Wu, Hema Vasavada, Karen K Hirschi, and Christopher S Chen. A non-canonical Notch complex regulates adherens junctions and vascular barrier function. *Nature*, 552(7684):258–262, dec 2017.